Ilmenau University of Technology

and

Institute of Communications and Navigation,
German Aerospace Center (DLR)

Master Thesis

Haider Abdulkarim

Comparison of Proposals for the Future Aeronautical Communication System LDACS

Supervisors:	Prof. Dr.-Ing. Giovanni Del Galdo
	Dipl.-Ing. Ulrich Epple, Dr.-Ing. Michael Schnell
Faculty:	Electrical Engineering and Information Technology
Research Group:	Digital Broadcasting Research Laboratory
Date:	6 December 2012

---

urn:nbn:de:gbv:ilm1-2013200010

Abstract

For meeting future capacity requirements in aeronautical communications, a new air-ground data link is needed. The European organization for the Safety of Air Navigation, EUROCONTROL, funded the development of two proposals for such a system. The first proposal, called LDACS1, is a digital broadband OFDM-based system, which was developed at the Institute of Communications and Navigation, DLR. The second proposal, LDACS2 is developed by a project team consisting of EGIS AVIA, Helios, SWEDAVIA and others. LDACS2 follows a single-carrier approach with GMSK modulation. Both systems intend to operate in the aeronautical part of the L-band (960-1164 MHz). However, this frequency band is already utilized by different aeronautical legacy systems, such as civil navigation aids DME or military communication systems (joint tactical information distribution system, JTIDS). Furthermore, LDACS is exposed to airborne co-site interference. A crucial issue in the selection process for one of the LDACS systems is to guarantee the co-existence between LDACS and the legacy systems. On the one hand, it has to be verified that LDACS has only minor influence onto the legacy systems. On the other hand, a reliable operation of LDACS in the presence of interference has to be guaranteed.

In this master thesis, the performance of LDACS2 is analyzed. This task comprises some theoretical considerations for investigating system features like capacity, spectral efficiency, scalability, and the possible number of simultaneous users. The results show the limitation of the offered bit rates per users due to the limited system bandwidth. However, for low-to-moderate bit rates user demands, the offered bit rates are within acceptable ranges. The main part of this work comprises the implementation of the LDACS2 system according to the specification in the simulation software. This covers the entire physical layer and the basic parts of higher layers. Special emphasis is put on the implementation and evaluation of effective channel equalization algorithms and channel coding schemes. Apart from AWGN channels, realistic aeronautical channel models are also applied. It turns out that the particular channel coding schemes, proposed in the specification, are not sufficiently robust. Other coding schemes that are more suited for such channel conditions are proposed and show large enhancements in the overall system performance. In addition, the robustness of LDACS2 against interferers from other aeronautical system, the DME, is investigated. The study shows that

LDACS2 system performs well against this type of interference for low-to-moderate interference duty-cycles. On the other hand, interference from LDACS2 on a DME system is negligible due to the relatively low transmission power of the LDACS2 compared to the DME interrogator. The final task is to compare LDACS2 to LDACS1 in terms of performance.

Acknowledgment

After completion of my Master thesis I wish to express my sincere gratitude to my supervisor Professor Dr. Giovanni Del Galdo for his continuous support and Dr. Alexander Ihlow and Mario Lorenz for their patient reviewing of this work. A special thank goes to my mentor Dipl. Ing. Ulrich Epple who continuously supported and advised me during the research period and also for his patience in reviewing the thesis afterwards.

I also would like to express my particular gratitude to the German Academic Exchange Service (DAAD), who made my dream come true by granting me a scholarship to pursue my master studies in Germany. The DAAD family continuously supported me in a friendly manner. They introduced me to the German life and culture and made me feel like living in my home country.

My gratitude goes also to the German Aerospace Center (DLR) and all the wonderful colleagues and the administration there, who made me feel at home in Bavaria and inspired me with their knowledge.

Studying in the university of Ilmenau was a great experience and source of enrichment. Thanks to all my Professors for their interesting courses they offered us, which I definitely will gratefully remember.

I dedicate my work to my mother and father, who never stopped motivating and stimulating me. They were supportive and extremely caring for me. They made it possible for me to acquire the best education. Though my thanks might not suffice, I hope that I will be able to do something for them in return one day.

Last, but by no means least, I would like to thank my brother, my friends in Iraq, at TU Ilmenau, in the lovely city of Munich, in Germany and the rest of the world. They gave me support and encouragement and inspired me to keep learning. A special thanks goes to Frau and Herr Doerr. When living with them in Seefeld, I experienced the most kindness and generosity.

Contents

1 Introduction **1**
1.1 Background and State of The Art . . . 2
1.2 Methodology . . . 3
1.3 Aeronautical Communication Demands . . . 4
1.3.1 LDACS2 Layers . . . 5
1.3.2 LDACS2 Physical Layer Specifications . . . 6
1.3.3 LDACS2 MAC Sublayer Specifications . . . 9
1.4 LDACS2 Air Interface . . . 12
1.4.1 Radio Frequencies . . . 13
1.4.2 Channel Bandwidth . . . 14
1.4.3 Co-channel spacing between near ACs . . . 15

2 LDACS2: The Transmitter **16**
2.1 Channel Coding, Interleaving and Multiplexing . . . 16
2.2 GMSK Modulation in Theory . . . 17
2.3 GMSK Modulation . . . 19

3 Aeronautical Channel Models **25**
3.1 Channel Modeling . . . 25
3.2 Aeronautical Channel Characterization . . . 28
3.2.1 En-route . . . 30
3.2.2 Taking-off/Landing . . . 32
3.3 Interference from Legacy Systems . . . 33

4 LDACS2 Receiver **35**
4.1 GMSK Demodulation . . . 35
4.1.1 Channel Estimation . . . 38
4.1.2 Matched Filter . . . 41
4.1.3 Maximum Likelihood Sequence Estimator (MSLE) . . . 41

4.1.4 The Viterbi Algorithm in the LDACS2 Receiver 43
4.2 Mitigating Fading Channel Effects 45
4.2.1 Forward Error Correction 46
4.2.2 Interleaving 48

5 LDACS2 Performance and Capacity 51
5.1 LDACS2 Performance under Aeronautical Channel Models 51
5.1.1 LDACS2 Simulator 51
5.1.2 LDACS2 Performance in AWGN 52
5.1.3 LDACS2 Performance in ENR Channel 58
5.1.4 LDACS2 Performance in the the TMA Channel 62
5.1.5 DME Co-site Interference 65
5.1.6 Time and Frequency Error Performance 66
5.2 LDACS2 Capacity 68
5.3 LDACS2 vs. LDACS1 Performance 70
5.3.1 LDACS1 Parameters 70
5.3.2 Performance Comparison 72

6 Conclusions 75
6.1 Implementaion 75
6.2 Results 76
6.3 Design Drawbacks 77
6.4 Future Work 77

Bibliography 83

List of Figures 86

List of Tables 87

Erklärung 88

Theses of the Master Thesis 89

1 Introduction

The traditional aeronautical communication is using the very high frequency (VHF) band for more than 70 years for analog radio systems. However, this band is already saturated. Besides, the analogue communication itself does not serve best in terms of spectral efficiency and the offered capacity. Hence, the need to develop a more efficient system capable of coping with the increasing data traffic (and number of aircrafts) has launched the Future Communication Study (FCS) in 2002. The project is proposed by the National Aeronautics and Space Administration (NASA) and the European Organization for the Safety of Air Navigation (EUROCONTROL). At the end of this project, two candidates have been selected by the International Civil Aviation Organization (ICAO) for a future digital air-ground communication systems. Those candidates are L-band Digital Aeronautical Communications System, Type1 (LDACS1) and L-band Digital Aeronautical Communications System, Type2 (LDACS2).

In order to select the final system proposal, independent studies on both of the proposals have to be carried out. Also, the performance of the two proposals has to be tested against different scenarios (traffic load, number of users) as well as the effects of Additive White Gaussian Noise (AWGN) and fading channels on the performance of the system. The well-known figure of merit, Bit Error Rate (BER), is chosen to evaluate the system performance. In this work, the focus is put on the LDACS2 proposal because of its low bandwidth utilization and relatively simple system structure for both the transmitter and the receiver blocks.

In this chapter, a brief history on the development of LDACS2 as well as a summary about the related contributions is given. Then, an overview of the general LDACS2 physical layer parameters and specifications is given. Later, the Medium Access Control (MAC) layer structure is depicted in summary, highlighting the main parameters that are used in simulating LDACS2 transmitter and receiver in the Chapters 2 and 4, respectively.

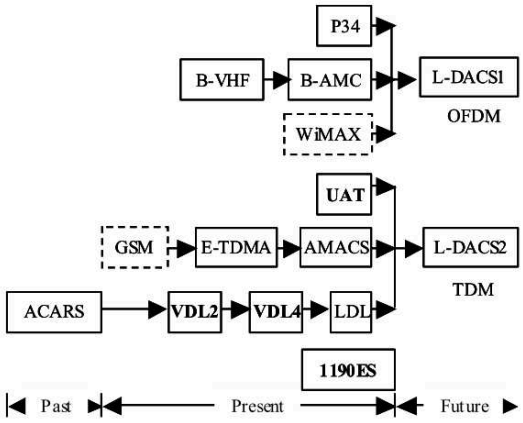

Figure 1.1: Evolution of aeronautical datalinks [4].

1.1 Background and State of The Art

Due to the tremendous air traffic increase in the last century, the need for more reliable and efficient communication between the aircrafts and ground stations emerged. Among other requirements, the need for data communication rather than only voice communication, higher data rates and better spectral efficiency are the most challenging burdens. In 2002, NASA and EUROCONTROL launched the project FCS to develop a new air-ground communication system capable to meet those emerging requirements [1]. The final selection by the ICAO voted for, among other candidates, two final proposals. Those are LDACS1 and LDACS2. They will be operated in the L-band (960 - 975 MHz), which is currently used by the Aeronautical Radio-navigation Services (ARS). The finally selected candidate is to be deployed in the year 2020. While LDACS1 is based on Frequency Division Multiple Acces (FDMA), LDACS2 is a Time Division Multiple Access (TDMA) system. LDACS2 is evolved from All Purpose Multichannel Aviation Communication System (AMACS), which is in turn derived from the well known GSM system, as shown in Figure 1.1.

The selection process of the final LDACS system proposal is shown in Figure 1.2 [2]. Although the testing and evaluation phase of the selection process is important, very few contributions have been made to this field. In [1], for example, the authors study the impact of LDACS on legacy systems that still work in L-band. The authors finally conclude that the interference from LDACS2 will be higher than that of LDACS1. In [3], the authors characterize the interference sources. They study the detection and mitigation techniques for LDACS1 only but not for LDACS2.

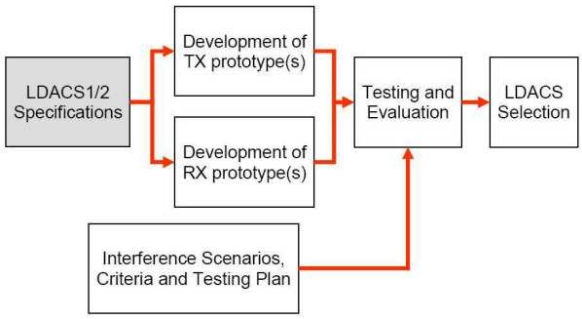

Figure 1.2: Selection process of the final LDACS proposal [2].

In [4], an independent theoretical comparison between the two proposals is provided. The comparison is done in terms of scalability, spectral efficiency, type of data traffic offered (symmetric vs. asymmetric) and possible interference from GSM base stations. However, their comparison is based not on simulation scenarios, but only on theoretical aspects. For the sake of independent comparison, our work presents an intensive study, implementation and evaluation of the proposed LDACS2.

1.2 Methodology

This work investigates the LDACS2 specifications and performance of the physical layer and MAC sublayer. In the following sections of Chapter 1, LDACS2 layers as summarized. The focus is made on the physical and MAC layers because of their influence on the system performance. In Chapter 2 the LDACS2 transmitter is described. The first contribution of this thesis is the implementing and validating of the LDACS2 transmitter. Then, the proposed channel coding are mentioned in brief. In Chapter 3 the channel models are introduced. Then, the commonly used aeronautical channel models are categorized. Afterwards, the DME system is described. The outcome of Chapter 3 is essential in evaluating the LDACS2 performance.

The other main contribution of this thesis is the implementation of LDACS2 receiver, as described in details in Chapter 4. Since the LDACS2 specifications do not describe the implementation of both the transmitter nor the receiver, large efforts have been dedicated to implement the LDACS2 simulator, taking the strict LDACS2 specifications into account. The concrete system model is then illustrated and the implementation issues are discussed in details. Special techniques to overcome implementation issues are also discussed. The channel coding and decoding are briefly discussed at this chap-

ter, with special emphasize on the coding parameters that directly affect the channel coding performance.

The other major contribution of this master thesis is presented in Chapter 5. In this chapter, the aeronautical channel models presented in Chapter 3 are adapted into the LDACS2 simulator. Then, the LDACS2 performance is evaluated under those channel models. Based on the system performance, more efficient channel coding parameters are suggested and validated which shows a considerable improvement in the performance. Besides, modifying the frame structure to cope with rapid fading channels is also proposed and validated through results. The LDACS2 reliability against timing and frequency error is tested and the results are presented. Finally, a comprehensive study on the practical LDACS2 capacity and actual information bit rates is presented.

1.3 Aeronautical Communication Demands

In this section the following two questions are answered: what kind of information does the aeronautical communication support? and what are main the challenges in aeronautical communication air-ground data-links?

To answer the first question, it is mandatory to consider the increasing demand for air traveling. As a consequence, the demand to maintain vital services to the airliners is increased. Among those services, Air Traffic Control (ATC) is the most important one. With ATC services, it is possible to control the traffic of the increasing number of aircrafts and to avoid collisions. Besides, other vital information are supported to the pilots, including weather informations, navigation and flight orders within the airport. Airline Operational Control (AOC) data maintains real-time traffic managements of hundreds of aircrafts and thousands of crew members to avoid delays and cancellation [6]. Obviously, for ATC and AOC data services, there are strict latency requirements (in the range of ms) and a certain probability that those messages are successfully transmitted.

Taking into consideration the speeds at which the airplanes cruising, there are basically two main dissimilarities between aeronautical communication links and land communication links. The first one is the long distances (large cell sizes) that need to be covered [4]. Considering the widely implemented IEEE 802.11 standard (WIFI) as an example, its coverage area is limited. Even the IEEE 802.16 (WiMAX) can only serve

up to 3 km in suburban areas. On the other hand, aeronautical data-links should cover up to 360 km, which makes the implementation of WiMAX unpractical. The second major difference is the speed of the aircraft. While WiMAX is designed to support a maximum velocity of up to 120 km/h, the cruising speed of a 747 airliner would be in the range of 900 km/h, resulting in a very high Doppler spread which reduces the spectral efficiency, as seen in Chapter 3.

As a conclusion, it is not feasible to use the existing ground communication technologies for aeronautical communications. However, LDACS2 makes use of some of the favorable features of existing technologies and adapts them accordingly. The LDACS2 is designed to be configured with flexibility in mind. That is, LDACS2 can serve point-to-point services (aircraft-to-aircraft or aircraft-to-ground station) as well multi-cast services (ground station-to-aircraft). In the current specifications, the focus is made on aircraft-to-ground and vise versa, with the possibility of extension to aircraft-to-aircraft in the future.

After selecting the final LDACS proposal, the old radios have to be kept at the beginning. There will be a step by step superseding of the old system. For example, the old VHF is still used for voice and LDACS for data (and also voice later on). Time path, however, is not yet clear, and probably it will be introduced between the years $2020 - 2030$.

1.3.1 LDACS2 Layers

In this section, the LDACS2 layers are discussed, with focusing on the layers that are related to this work. Since the performance of LDACS2 depends on the physical and MAC layers, this work focuses on those layers. It should be mentioned that voice services will also be supported, but its implementation is not yet specified in the specifications.

The general LDACS layers are illustrated in Figure 1.3. The physical layer, as the name suggests, deals with all transmission concepts as well as the channel coding. The MAC sublayer defines the framing structure of LDACS2 and time synchronization. The Data Link Sublayer (DLS) relies on the MAC sublayer to ensure that the user messages are delivered without errors through establishing and releasing of DLS connections. The offered connections are connection-oriented (point-to-point) and connectionless (broadcast services). The LDACS2 Service Sublayer (LSS) provides flexible

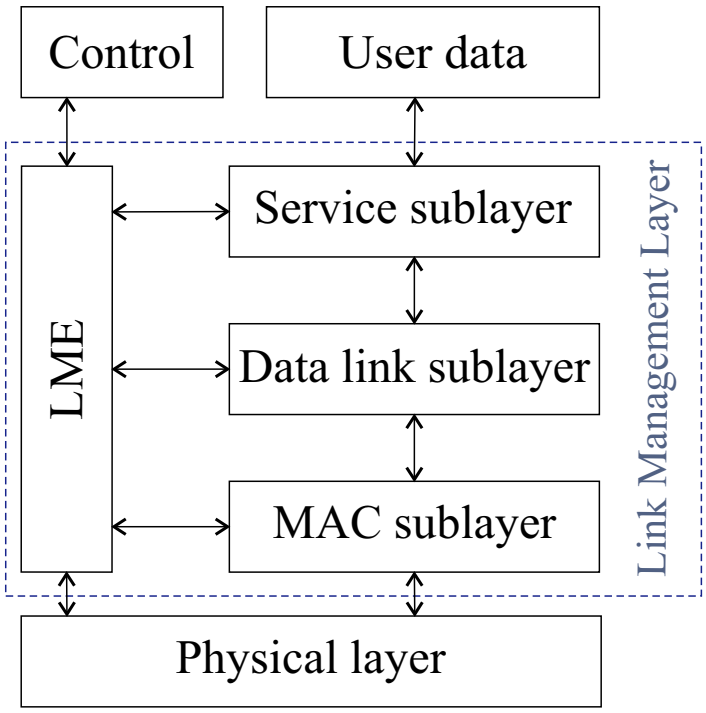

Figure 1.3: LDACS2 layers.

burst formatting for the MAC sublayer framing structure and is also responsible of the transmission and reservation protocols over the MAC sublayer. Finally, the Link Management Entity (LME) is responsible for establishing and maintaining the connections.

The entities MAC, LSS, DLS and LME together represent the Link Management Layer (LML), which is also responsible for the login and handover mechanisms. Since the performance of the physical layer and MAC sublayer determines the overall performance of LDACS2, this work focus on the physical and MAC entities. However, the other sublayers functions are described in details in [2].

1.3.2 LDACS2 Physical Layer Specifications

In this section, the physical layer highlights of LDACS2 are demonstrated. It was adapted from the AMACS. LDACS2 is operated in the lower part of the L-band, namely $960-975$ MHz, as shown in Figure 1.4. The standard [2] inherits some features from its ancestors, see Figure 1.1. For example, the Time Division Duplexing (TDD) is adopted from AMACS. Besides, the principle of dedicated and on-demand slots is extended from AMACS to LDACS2. The tendency to operate in a less congested

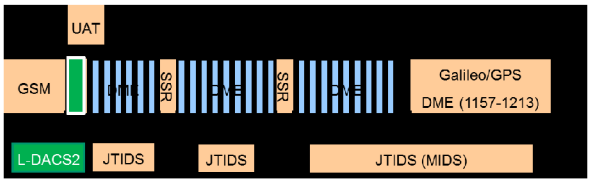

Figure 1.4: L_band spectrum usage.

spectrum is also attained from the L-band Digital Link (LDL). LDL is the L-band version of the VHF Digital Link (VDL) with two variants: VDL2 and VDL4.

Because LDACS2 is to be implemented in the lower part of L-band, it will cause out-of-band interference to other systems, like the GSM. Thus, the LDACS2 bandwidth is limited to 200 kHz, with a gross bit rate R_b of 270.833 kbps/channel. The modulation scheme is chosen to be Gaussian Minimum Shift Keying (GMSK), which is similar to Minimum Shift Keying (MSK) modulation. To understand GMSK, MSK is recalled first. MSK is based on Quadrature Phase Shift Keying (QPSK). However, MSK uses half sine wave instead of squared pulse to represent the bit. The resulting signal is a constant modulus signal. Further, the quadrature-phase component (Q) is delayed by half the QPSK symbol time T_s with respect to the In-phase component (I). The signal phase is then continuous and linear which reduces the out-of-band radiation extending out of the carrier frequency f_c experienced in PSK. Besides, MSK is a constant amplitude modulation. As a consequence, the MSK signal is more robust against amplitude fading and attenuation. In GMSK, the modulation index m is set to 0.5. The bit time T_b is defined as

$$T_b = \frac{T_s}{2}. \tag{1.1}$$

The relation between T_s and R_b is given by

$$\frac{T_s}{2} = \frac{1}{R_b}, \tag{1.2}$$

then T_b is defined as

$$T_b = \frac{1}{R_b} = 3.69\ \mu\text{s}. \tag{1.3}$$

The name MSK comes from the fact that MSK could be seen as a form of Frequency Shift Keying (FSK) with frequency deviation Δ_f defined as [7]

$$\Delta f = f_1 - f_2, \tag{1.4}$$

where f_1 and f_2 are the two LDACS2 frequency components after modulation. To be able to recover the data at the receiver side, Δ_f should be

$$\Delta f = \frac{1}{2T_s} = \frac{R_b}{4}. \tag{1.5}$$

(1.5) states that the minimum shift in frequency should be $R_b/4$ to recover the signal without ambiguity, and hence the name *minimum shift keying*.

In LDACS2 the resulting frequency components can be written as

$$\begin{aligned} f_1 &= f_c + \tfrac{R_b}{4}, \\ f_2 &= f_c - \tfrac{R_b}{4}. \end{aligned} \tag{1.6}$$

This is equivalent to have f_c swinging between two values, as seen in Figure 1.5. That is, a logical 1 increases the phase by 90° over T_b while a logical 0 decreases the phase by 90°.

The modulation index m is then related to T_s by [8]

$$m = \Delta f T_s = 0.5\ . \tag{1.7}$$

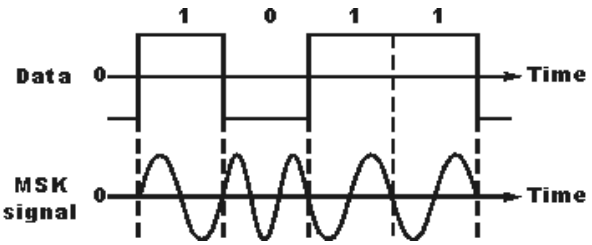

Figure 1.5: MSK modulated signal [5].

To further limit the system bandwidth B in GMSK, the MSK output signal is filtered with a Gaussian low pass filter. B is then limited to 200 kHz and the resulting spectrum decays faster after the system bandwidth than that of the MSK spectrum. However, since B is smaller than R_b, Nyquist sampling theorem is violated. As a result, Inter Symbol Interference (ISI) is introduced in the signal. This ISI is easily mitigated at the receiver, as seen in Chapter 4.

LDACS2 specifies the normalized-bandwidth-time product BT to be 0.3, according to [8]

$$BT = \frac{f_{3dB}}{R_b} = 0.3, \tag{1.8}$$

where f_{3dB} is the Gaussian filter one-sided bandwidth, which is equal to 81.25 kHz.

The LDACS2 transmit output power is set to 350 W at the ground station and 50 W at the aircraft. After link budget calculations [2], the maximum radius of LDACS2 cell size is 200 Nautical Mile (NM), where 1 NM is 1.852 km.

1.3.3 LDACS2 MAC Sublayer Specifications

In this section the main features of the LDACS2 MAC layer are covered. The main architecture is adopted from the MAC layer of AMACS, with a fixed frame length of 1 s to accommodate high priority messages that should not be delayed. The frame structure is TDD in the sense that either one of the communicating entities (the transmitter or the receiver) is allowed to send or receiver at a given time. Each LDACS2 frame of 1 s is divided into five sections, namely UP1 and UP2 for the up-link, CoS1 and CoS2 for the down-link and the LoG2 section for logging in. The frame structure

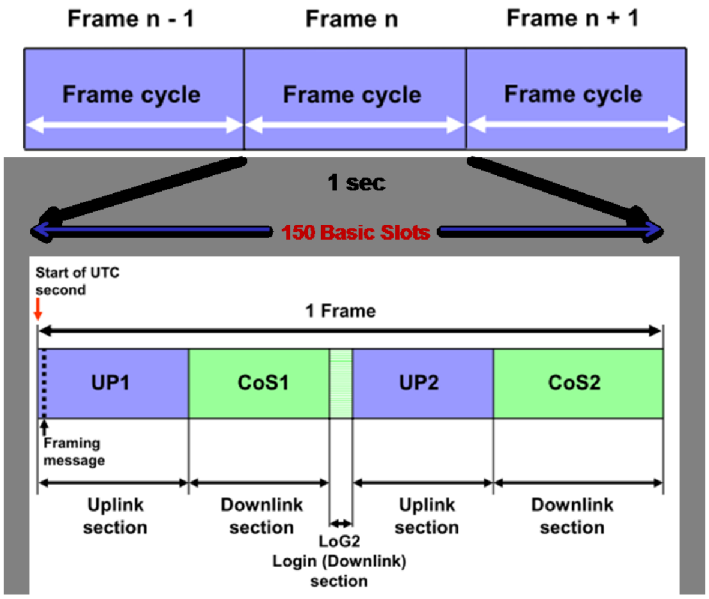

Figure 1.6: LDACS2 frame structure [2].

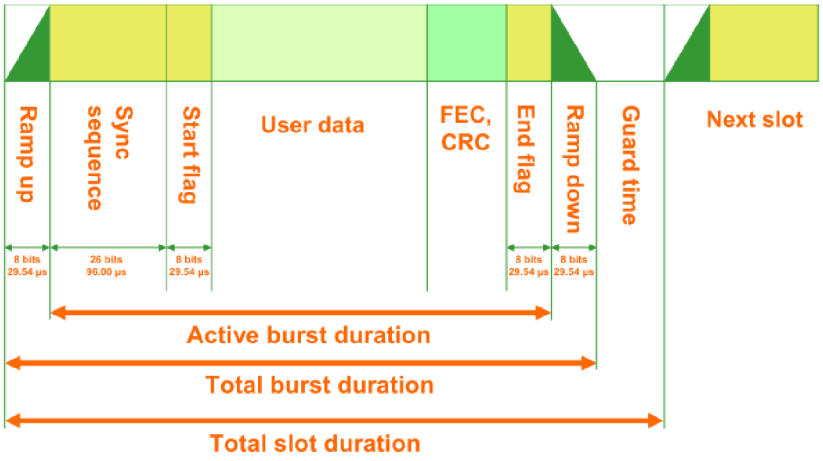

Figure 1.7: Basic slot structure [2].

is illustrated in Figure 1.6. It consists of 150 basic slots or equivalent size slots, with basic slot length of 6.666 ms. Each slot has its header, trailer, address, user data and guard time fields. In order to avoid the insertion of large guard time, accurate time synchronization between the Aircraft (AC) and the Ground Station (GS). However, guard time is only introduced at the end of the slot, since there is another guard period inserted in the preceding slot. The general structure of a basic slot is shown in Figure 1.7.

It is also possible that a slot is shorter than the basic slot. On the other hand, a burst spanning multiple basic slots is used whenever the message is longer than one slot or to contain multiple messages from the same user. Since there is one header and one trailer in a single burst, there is less overhead in a burst than in a slot.

The UP1 and UP2 sections are used to transmit data from the GS to the AC. The GS concatenates all of its messages into two continuous burst, one for each section. Since it has control of its entire UP section, the GS transmits in bursts rather than slots. Each UP burst spans a number of basic slots. That is, the minimum size of a UP burst is two basic slots (13.33 ms), see Figures 1.8. The CoS1 section is used to transmit high priority short messages from the AC to GS. The CoS1 slot (the slot in CoS1 section) length is 1.11 ms (see Figure 1.9). If a user needs access to bursts for long messages, it requests access to the CoS2 section during its assigned CoS1 slot and it would be granted access to one or more slots in CoS2 section. While a CoS1 slot is short, CoS2 slot has a length equivalent to the basic slot, see Figure 1.10. The log-in procedure takes place in the LoG2 section. With a duration of 3.33 ms, the LoG2 slot is used by the AC to have access to a CoS1 slot. The LoG2 slot structure is illustrated in Figure 1.11.

To provide the maximum flexibility, the length of each section can be changed dynamically according to the user demand. The total duration of the five sections is 1 s. However, only the GS is allowed to change the sections length. When it intends to modify the sections duration, the GS should notify all the logged-in aircrafts multiple times with sufficient frames before the actual change in the frame structure takes place; this is to ensure the high probability of all aircrafts to adapt to the new frame structure. A summary of the LDACS2 frame parameters is given in Table 1.1.

Table 1.1: LDACS2 frame parameters.

Parameter	Value
Frame length	1 s
Frame duration	150 basic slots
Slot Duration	6.666 ms (basic slot)
Bits / slot	1806 (basic slot)
Duplexing	half (uplink and downlink)

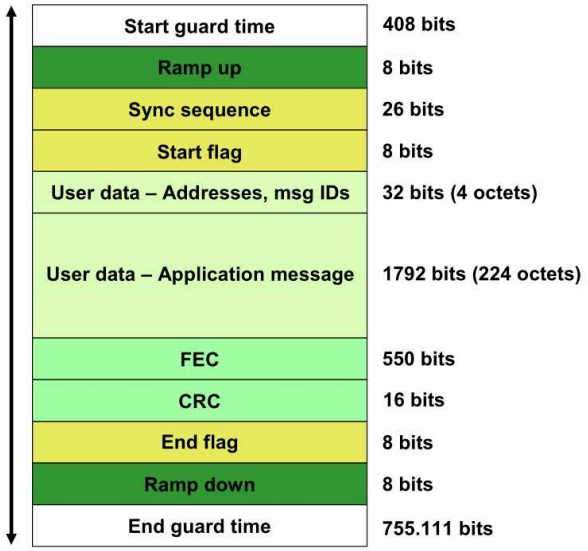

Figure 1.8: UP slot, 3612 bits, 13.33 ms [2].

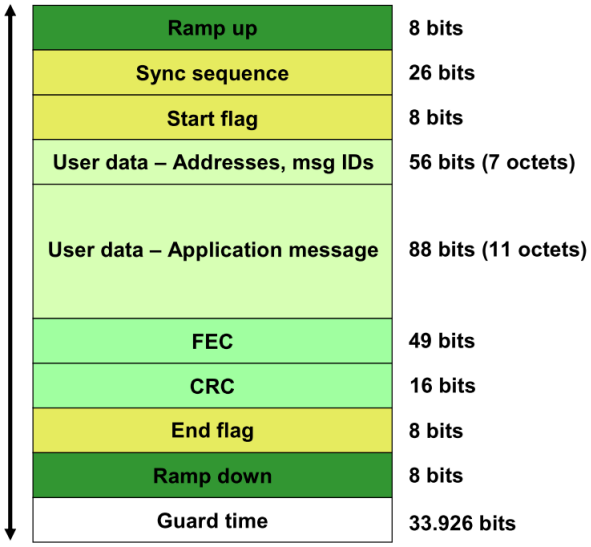

Figure 1.9: CoS1 slot, 300 bits, 1.11 ms [2].

1.4 LDACS2 Air Interface

In this section, a summary of the main LDACS2 transmission features is provided. The transmission characteristics cover the radio frequencies, channel bandwidth as well as the guard bands that should be maintained.

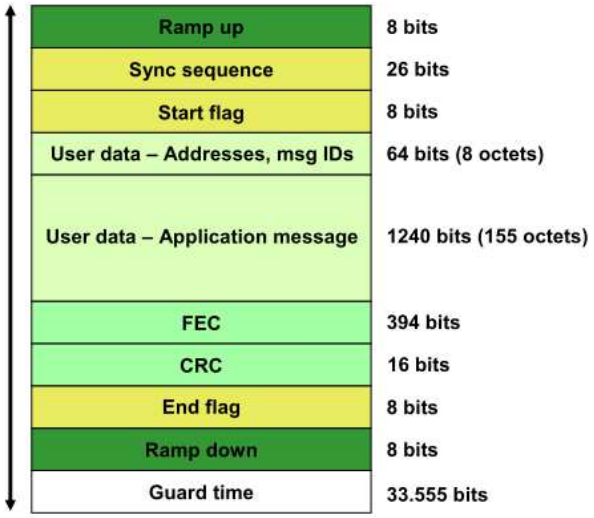

Figure 1.10: CoS2 slot, 1806 bits, 6.66 ms [2].

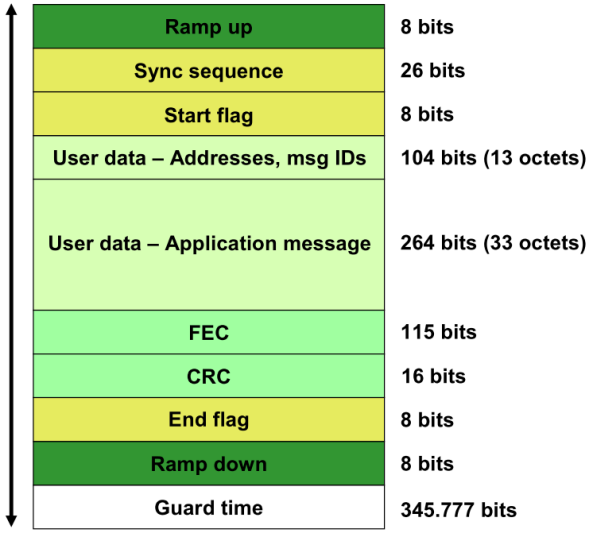

Figure 1.11: LoG2 slot, 902 bits, 3.33 ms [2].

1.4.1 Radio Frequencies

Although the assigned frequency ranges from 960 - 975 MHz, a guard band of 500 kHz at the lower edge of the spectrum should be maintained. This is to protect other communication systems that use the frequencies below 960 MHz (such as GSM systems) from LDACS2 out-of-band radiation.

Table 1.2: Channel bandwidth vs. various cell sizes.

Scenario	Service	No. of AC	User Demand	Channels required	Total bandwidth
TMA(large)	ATS and AOC	52	47 kbps	1	200 kHz
Enroute(medium)	ATS and AOC	64	55 kbps	1	200 kHz
Enroute(large)	ATS and AOC	204	188 kbps	2	400 kHz

1.4.2 Channel Bandwidth

The LDACS2 specification suggests a nominal channel bandwidth of 200 kHz. This is supposed to be sufficient to serve the most operational scenarios. However, when there is a need for more capacity per cell, channel aggregation should be used. When implemented, two or more channels, each with a bandwidth of 200 kHz, serve as a virtual single channel. This allows higher data rates to be achieved. Channel aggregation is achieved by using a frequency reuse concept (from the GSM) in adjacent cells, allowing more flexible frequency planning and saves frequency resources. The traffic load of the cell will be shared among the channels. One way to achieve this is to use cell segmentation (taken from GSM) by using sectorized antennas. An example of channel aggregation is illustrated in Table 1.2

The minimum channel separation between two channels belonging to the same cell should be at least 600 kHz to prevent interference between adjacent bands. However, considering the minimum clearance distance between the GS and the nearest AC, the minimum separation could be reduced to 400 kHz. Considering the example in [2]: with 200 kHz frequency separation, the two mobile stations have to be separated by 10 NM (approximately 18.5 km). With a channel separation of 400 kHz, the AC receiver is still able to demodulate the signal from the GS. In this case the two mobile stations (considering two ACs) have to be separated by 0.23 NM (approximately 0.42 km), which is far less the minimum allowable separation between any two ACs at a given time.

1.4.3 Co-channel spacing between near ACs

In this section, the case of two ACs working at the same channel frequency, but in two different (adjacent) cells is considered. In this case AC1 is transmitting to GS1 while AC2 is receiving data from GS2. The goal is to determine the minimum distance between the two ACs that lead to a successful demodulation of the received signal at both of the ACs. The minimum spacing is found to be 80 NM to keep the Carrier to Interference (C/I) at a maximum of 9 dB, according to Table 1.3 [2].

Table 1.3: Channel interference.

Interference Type	Interference Ratio
co-channel interference	9 dB
adjacent (200 kHz) interference	−9 dB
adjacent (400 kHz) interference	−41 dB
adjacent (600 kHz) interference	−49 dB

2 LDACS2: The Transmitter

The LDACS2 specification retains some features from GSM: the reason behind this is to simplify the physical implementation by using already existing technologies in the market. This will help the developers to migrate to faster data rate services such as EDGE or GPRS whenever higher traffic densities and increasing traffic demands are desired. This chapter concisely reveals the LDACS2 transmitter structure, shown in Figure 2.1. First, a brief description of the coding parameters suggested by the specifications is listed. Then, an introduction into GMSK is presented and compared to MSK. Later, the basic GMSK modulation steps are presented according to the international GSM standards. The GMSK modulation is then used implementing the LDACS2 transmitter using MATLAB simulation environment.

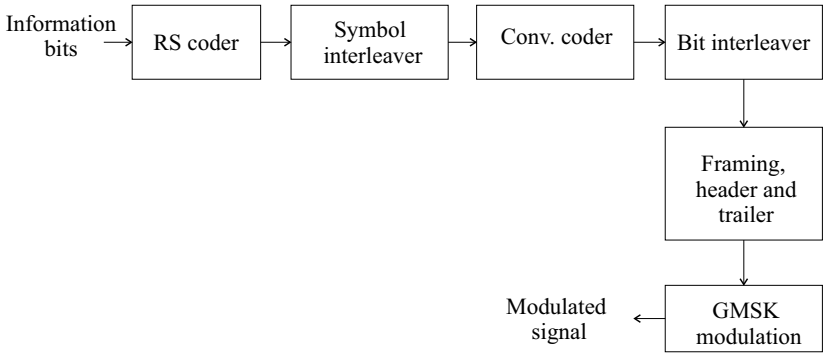

Figure 2.1: LDACS2 general transmitter structure.

2.1 Channel Coding, Interleaving and Multiplexing

To protect the transmitted data against random and burst channel errors, channel coding is used. The LDACS2 specification [2] specifies a concatenated coding scheme to be used. It consists of inner and outer codes. The inner code is a convolutional code $(7, 171, 133)$, where 7 is the constraint length. This code has been already implemented

in DVB systems. It makes the transmitted signal robust against AWGN random errors. The chosen code rate $R_c = 3/4$, which is accomplished using puncturing from a mother $R_c = 1/2$ code. The outer coder is a Reed Solomon (RS) code. The specification suggest the usage of RS$(15, 11, 4)$ or RS$(31, 23, 5)$. Between the two codes, a block or diagonal interleaver exists. A bit interleaver is used after the inner coder to randomly permute the convolutional-coded bits. This protects the bits against uncorrelated errors over time. A comprehensive study on the coding and interleaving techniques is presented in Section 4.2.

The multiplexing step simply accumulates the bits into a stream formatting prior to the modulation step. This also includes attaching the flag bits (message type), ramp bits (to reduce out of band emission), training sequence, Code Redundancy Check (CRC) and guard bits. The guard bits length is equal to the maximum propagation delay between the transmitter and the receiver. This maximum length is calculated based on a maximum cell radius of 200 NM.

2.2 GMSK Modulation in Theory

As stated in Chapter 1, the GMSK modulation scheme is chosen as the proposed modulation scheme for LDACS2. GMSK is a special form of MSK. The goal of MSK modulation is to limit the maximum carrier phase transition between successive symbols to $\pi/2$. As a result, there are no abrupt phase transitions, implying that the MSK spectrum is band limited. To understand the GMSK modulation, the MSK modulation is first considered. The MSK modulated signal, $s_i(t)$ could be written as [12]

$$s_i(t) = a_i \cos\left(\frac{\pi t}{T_s}\right) \cos(2\pi f_c t) + b_i \sin\left(\frac{\pi t}{T_s}\right) \sin(2\pi f_c t), \tag{2.1}$$

where a_i and b_i are Non-Return-To-Zero (NRZ) input bits, T_s is the symbol duration, in seconds. The relationship between the I and Q components of MSK modulation is seen in Figure 2.2.

Because of the $T_s/2$ s delay between a_i and b_i (Figure 2.3), only one of them can change at a time. The effect of the term $a_i \cos(\pi t/T_s)$ is to force the carrier term $\cos(2\pi f_c t)$ to go to zero at the bit transition point (end of T_b) while the other carrier term $\sin(2\pi f_c t)$

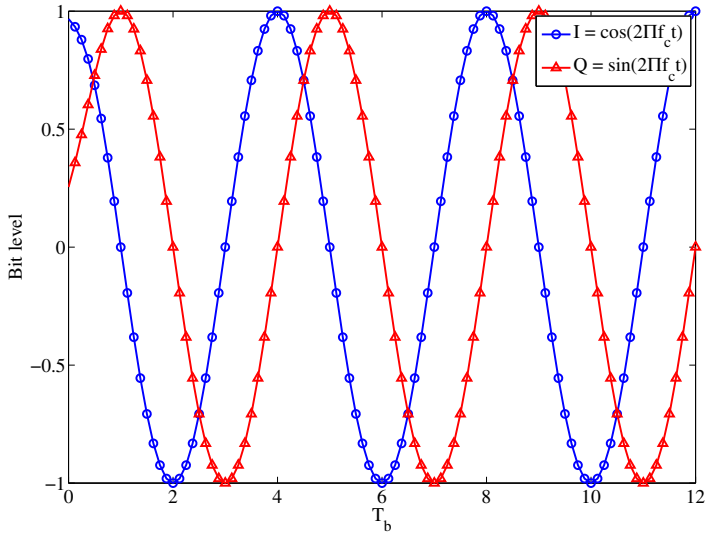

Figure 2.2: MSK modulator fed with a sequence of ones. I lags Q by $\pi/2$. Each T_b increases the phase by $\pi/2$.

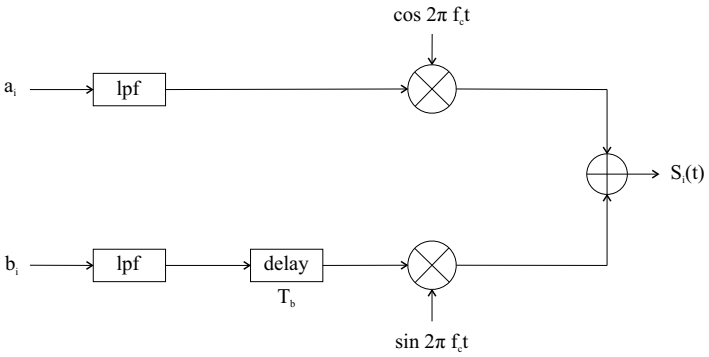

Figure 2.3: MSK modulator.

is at its peak. The same discussion applies when the carrier $\cos(2\pi f_c t)$ is at its peak while the other carrier term $\sin(2\pi f_c t)$ is forced by the term $b_i \sin(\pi t/T_s)$ to go to zero.

f_c is chosen such that it has integer number of half cycles within each T_s. This assures no phase discontinuity at the bit transition point.

Using trigonometry, (2.1) is rewritten as

$$s_i(t) = \begin{cases} \cos\left(2\pi f_c t \mp \frac{\pi t}{T_s}\right) & \text{for } a_i = 1,\ b_i = \pm 1, \\ \cos\left(2\pi f_c t \pm \frac{\pi t}{T_s} + \pi\right) & \text{for } a_i = -1,\ b_i = \pm 1. \end{cases} \tag{2.2}$$

Equivalently

$$s_i(t) = \cos\left(2\pi f_c t - \frac{a_i b_i \pi t}{2T_b} + \theta\right), \tag{2.3}$$

where

$$\theta = \begin{cases} 0, & \text{for } a_i = 1, \\ \pi, & \text{for } a_i = -1. \end{cases} \tag{2.4}$$

From (2.4), one concludes that since either a_i or b_i changes every T_b while the other is kept constant, the maximum phase difference is limited to $\pi/2$, as seen Figure 2.4.

Recalling (1.5), the minimum frequency separation Δf between two adjacent carriers is $R_b/4$, in order for the synchronous detector at the receiver to detect the signal without ambiguity.

In GMSK modulation, it was decided [13] to further limit the bandwidth of the base-band pulse train by filtering the signal with a pre-modulation filter (Gaussian Filter). The resulting output phase is very smooth compared to that of the MSK (Figure 2.4). As a consequence, the GMSK occupied bandwidth B is narrower than that of MSK (Figure 2.5). A comprehensive description of the GSMK modulation steps is given in Section 2.3.

2.3 GMSK Modulation

A comprehensive description of the GSMK modulation steps is given in this section. Following the GSM specification [9], there are basically four steps to modulate the data bits (baseband representation is considered):

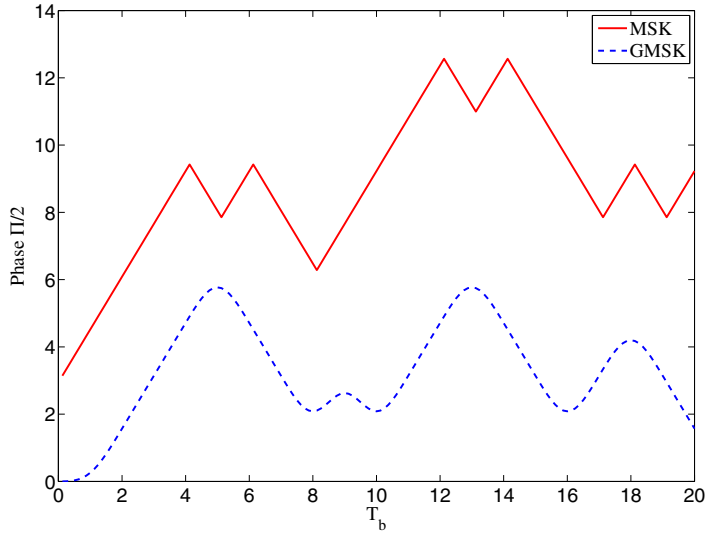

Figure 2.4: For the same binary sequence, GMSK phase is smoother than MSK.

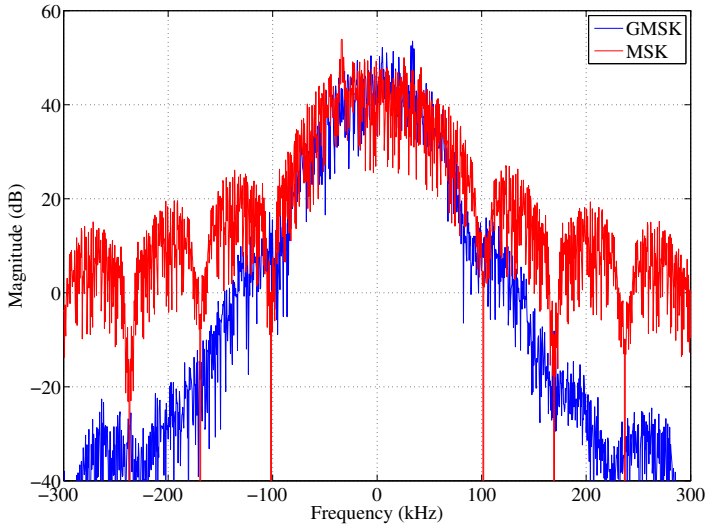

Figure 2.5: GMSK vs. MSK Spectrum. High attenuation for GMSK spectrum after 200 kHz.

- **Differential Encoding**

  The data bits d_i to be modulated are in the Return-to-Zero (RTZ) form ($d_i = [0, 1]$). They are differentially encoded, to obtain $\hat{d}_i$

$$\hat{d}_i = d_i \oplus d_{i-1}, \text{ where } d_i \in \{0, 1\}. \tag{2.5}$$

Then the input to the modulator becomes

$$a_i = 1 - 2\hat{d}_i, \text{ where } a_i \in \{-1, 1\}. \tag{2.6}$$

Note: the GSM specification assumes an infinite sequence of ones preceding the actual burst start.

- **Filtering**

  The output from the differential encoder a_i, passes a Gaussian filter, whose impulse response $g(t)$ is given by

$$g(t) = h(t) * \text{rect}\left(\frac{t}{T_b}\right), \tag{2.7}$$

where $*$ denotes a convolution. And

$$\text{rect}\left(\frac{t}{T_b}\right) = \begin{cases} \frac{1}{T_b} & \text{for } |t| < \frac{T_b}{2}, \\ 0, & \text{otherwie.} \end{cases} \tag{2.8}$$

$h(t)$ is defined as:

$$h(t) = \frac{\exp\left(-\frac{t^2}{2\sigma^2 T^2}\right)}{\sqrt{2\pi}\sigma T_b}, \tag{2.9}$$

given

$$\sigma = \frac{\sqrt{\ln(2)}}{2\pi B T_b}. \tag{2.10}$$

For GSM, as well as LDACS2 B is the 3dB bandwidth of the filter $g(t)$, given by:

$B = 81.25$ kHz and $T_b = 3.69$ μs.

- **Modulated Signal Generation**

  The output signal $x(t)$ from the filter $g(t)$ is described as

$$x(t) = \sqrt{\frac{2E_c}{T_b}} \cos(2\pi f_c t + \phi(t) + \phi_0), \tag{2.11}$$

  where E_c is the energy per modulating bit, $\phi(t)$ is the phase function and ϕ_0 is a random phase (constant during T_b).

- **Phase Function**

  The phase function $\phi(t)$ is defined as

$$\phi(t) = \sum_i a_i \pi h(t) \int_{-\infty}^{t-iT_b} g(u)\, du. \tag{2.12}$$

Since the ideal shaped Gaussian filter has an infinite bandwidth, it is not be realizable in practice [10]. Instead, a practical approximation is to limit the time response of the filter to a length of L, where $L \geq 3$ is the number of samples per bit that represent the Gaussian pulse. For GSM (as well as LDACS2), it is decided to choose $L = 3T_b$, see Figure 2.6. That is, (2.7) is altered as

$$\acute{g}(t) = g\left(t - \frac{LT_b}{2}\right) w_l(t), \tag{2.13}$$

where $w_l(t)$ is the windowing function used to limit the impulse response of the filter $g(t)$ to $3T_b$, defined as

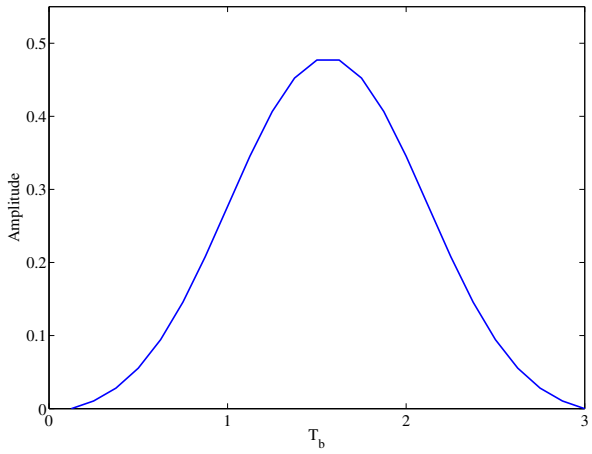

Figure 2.6: Pulse shaping function $\acute{g}(t)$ is limited to $3T_b$.

$$w_l(t) = \begin{cases} 1 & \text{for } 0 \leq t \leq LT_b, \\ 0 & \text{otherwise,} \end{cases} \tag{2.14}$$

A closer look at (2.13) indicates that ISI is intentionally introduced into the signal. This is because the symbol is now spread over a $3T_b$ period instead of $1T_b$, see Figure 2.6.

However, this kind of ISI can be easily mitigated by using a Maximum Likelihood Sequence Estimator (MLSE) equalizer at the receiver, as explained in Chapter 4.

In this work, the described GMSK modulator is implemented and tested using MATLAB simulator. This GMSK modulation approach was chosen based on LDACS2 recommendation [2]. The implementation also include the channel coding, intreleaving and the multiplexer. A comprehensive description of the coding and interleaving is introduced in Chapter 4. The multiplexer step adds the header and trailer bits to each user message, in order to construct the LDACS2 frame, as explained in Section 1.3.3.

The general LDACS2 transmission chain is demonstrated in Figure 2.7.

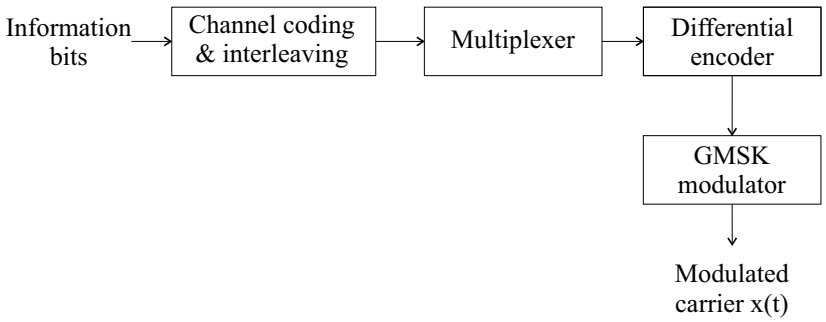

Figure 2.7: LDACS2 transmitter chain.

3 Aeronautical Channel Models

When studying communication systems, one of the most important factors to be considered is the transmission channel. The term ”channel” refers to the medium between the transmitter and the receiver. In its simplest form, the channel is considered ideal when the transmission occurs in the free space. That is, the free space path loss model is assumed whenever there are no obstacles between the transmitter and the receiver. In reality, the experienced channel effects are far from being ideal. Those effects are caused by the relative motion between the transmitter and the receiver as well as the existence of obstacles in between. Those obstacles introduce the so called multi-path fading. The received signal level, attenuated by the path loss, additionally degrades by the multi-path effect.

In this chapter, a brief introduction to the general wireless channel models is made. Then, the experienced aeronautical channel models are characterized with a summary of each channel model parameters. The outcome of this chapter will facilitate studying and simulating the LDACS2 performance.

3.1 Channel Modeling

In this section, the free space path channel model is introduced. Then, channel fading and multi-path effect is explained. The concept of channel modeling is then summarized. The simplest form of the channel model assumes that the received signal is only attenuated by the traveled distance and AWGN. The AWGN channel model is assumed whenever the noise samples are statistically independent and follow a complex Gaussian distribution with mean μ and standard deviation σ for both I and Q components. The AWGN is generated at the receiver, basically due to the thermal noise at the normal operation temperature. The Power Spectrum Density (PSD) of the

AWGN is constant which indicates that the noise is added up equally to all frequency components of the original signal.

In addition to this added noise and following the simplest channel model, the free space path loss model is assumed whenever there are no obstacles between the transmitter and the receiver. Furthermore, the received signal does not suffer from reflection, diffraction or scattering phenomena. Usually, this channel model is described by the free space path loss L_s factor as follows

$$L_s\left(d\right) = \left(\frac{4\pi d}{\lambda}\right)^2, \tag{3.1}$$

where d is the distance between the transmitter and receiver, and λ is the wavelength of the carrier frequency f_c. As expected, $L_s(d)$ grows for large values of d, f_c, or both.

In reality, most of the wireless channels cannot be modeled by the simple free space path loss model. The reason is that besides the path attenuation, the receiver receives multiple copies of the original signal via different paths, which is known as multi-path propagation or fading. Those types of channel models are widely used in the modeling of communication channels because they can describe the channel characteristics efficiently.

There are mainly two types of fading:

1. **Large scale fading** : The fading occurs due to the relative motion between the transmitter and the receiver, because the transmitted signal suffers from being blocked by large building, hills, etc. The large scale fading (also called shadowing) is a function of d. The path loss $L_p(d)$ is described by the nth-power law [14]) as

$$L_p(d)(\text{dB}) = \overline{L_p}(d_0) + 10n\log\left(\frac{d}{d_0}\right), \tag{3.2}$$

where $\overline{L_p}(d_0)$ is mean path loss at the reference distance d_0 and n is the path loss exponent.

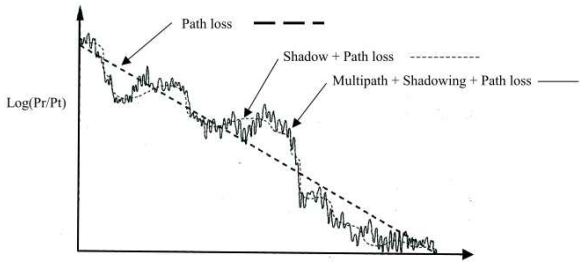

Figure 3.1: Large fading (shadowing) vs. small scale (multi-path) fading [14].

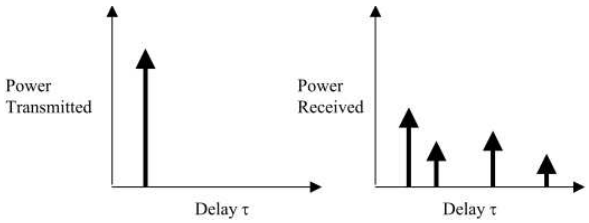

Figure 3.2: Multipath power delay profile example [14].

2. **Small scale fading**: The fading effect in this case is mainly due to the multi-path reflected versions of the signal, which vary in the phase and the amplitude. It is called small scale because of the large variation in the fading effect due to very small displacements (in terms of $\lambda/2$) when either the transmitter or the receiver moves. Due to the multi-path components, the total effect of the received signal components may vary between constructive and destructive. This is because of the variations in the phase of the multiple reflected components. The effect of both large and small scale fading is illustrated in Figure 3.1.

To simplify channel modeling, and since the received signal is actually the effective sum of the reflected replicas of the transmitted signal, the channel is often described as a multi-tap profile. Each received component is described by its relative arrival time and the intensity of the respective component, as shown in Figure 3.2.

The received signal consists of a single component lying at $\tau = 0$, which is the Line of Sight (LOS) component and further components lying at $\tau > 0$, where τ is the delay with respect to the LOS component. A useful description of the channel behavior is obtained from the maximum time after which the received component is negligible, which is called the maximum access delay, denoted by $\tau_{\max}$. A channel with large $\tau_{\max}$ is considered a dispersive channel while a channel with a very small $\tau_{\max}$ approaches a frequency flat fading channel. In Section 3.2, a description of the aeronautical channel models is introduced.

3.2 Aeronautical Channel Characterization

In this section the widely used aeronautical channel models are classified. The parameters describing the channel model are introduced. The outcome of this section is used in Chapter 5 to study the LDACS2 performance under various channel conditions. Following the discussion in Section 3.1 and due to the movement of the AC, the channel is a time-variant system. The channel impulse response $h(t, \tau)$ is a function of two variables, time t and delay τ. To stochastically describe the channel, a multi-dimensional joint pdf representation of the impulse response is required, which is a complex description. To simplify the channel description, the Autocorrelation Function (ACF) is used instead. The ACF, which describes the second order statistics, is defined for a time variant system as [29]

$$R_{hh}(t_1, t_2, \tau_1, \tau_2) = \mathbb{E}\{h^*(t_1, \tau_1)h(t_2, \tau_2)\}. \tag{3.3}$$

R_{hh} in (3.3) is a function of four variables, thus it is yet complicated to characterize the aeronautical channels. Hence, the assumption Wide-Sense Stationary Uncorrelated Scatterers (WSSUS) is often used [22]. WSS assumption states that the statistical channel properties do not change over time. That is the second-order amplitude statistics do not depend on the time instants t_1 and t_2 but rather on the time difference $\Delta t = t_2 - t_1$. Thus, R_{hh} could be written as [29]

$$R_{hh}(t_1, t_2, \tau_1, \tau_2) = R_{hh}(t_1, t_1 + \Delta t, \tau_1, \tau_2) = R_{hh}(\Delta t, \tau_1, \tau_2). \tag{3.4}$$

The channel WSS assumption has to be hold true for an arbitrary t. The US assumption states that the scatterers related to different delay paths (i.e. $\tau_1 \neq \tau_2$) are uncorrelated. The US can be described by Fourier transforming R_{hh} into the time frequency correlation function R_{HH} [29]. For R_{HH} to meet the US assumption, it has to fulfill

$$R_{HH}(t_1, t_1 + \Delta t, f_1, f_1 + \Delta f) = R_{HH}(\Delta t, \Delta f), \tag{3.5}$$

where f_1 is the frequency notch corresponding to τ_1.

The relative motion between the transmitter and the receiver causes frequency shifts in the received signal, which is described by the Doppler shift f_D. When the AC is moving towards the GS, the resulting f_D is positive and expressed as $f_c + f_\mathrm{D}$. On the other hand, f_D is negative when the AC is moving away from the GS, and the received frequency is $f_c - f_\mathrm{D}$. f_D is related to f_c and velocity V by

$$f_\mathrm{D} = \frac{V}{c} f_c, \tag{3.6}$$

where $c = 3.10^8$ m/s is the speed of electromagnetic waveform traveling in vacuum. f_D causes spectral broadening of the received signal spectrum, known as Doppler Power Spectrum $S(V)$, which is described by [22]

$$S(V) = \frac{1}{\pi f_\mathrm{D} \sqrt{1 - \left(\frac{V}{f_\mathrm{D}}\right)^2}}. \tag{3.7}$$

The width of the Doppler power spectrum is called the Doppler spread. The coherence time τ_c of the channel is described as the time during which $h(t, \tau)$ is approximately constant. If the symbol time T_s is very small compared to τ_c, the channel is said to be a slow fading channel. On the other hand, when T_s is comparable to the τ_c of the channel (up to $10\tau_c$), the channel is said to be a fast fading channel. The Doppler spread of the channel and τ_c are related by [22]

$$\tau_c \simeq \frac{9}{16\pi f_\mathrm{D}}. \tag{3.8}$$

In general, following the WSSUS assumption, the channel model can be described by the delay power profile and the Doppler power spectrum. Moreover, the relation

between the direct and the p-th scattered component is described by the Rician K-factor, K_{Rice} as [28]

$$K_{\text{Rice}} = 10 \log 10 \left(\frac{|d|^2}{\sum_{p=0}^{P-1} |a_p|^2} \right) \text{dB}, \tag{3.9}$$

where :

d: weight coefficient of the direct (LOS) component,
a_p: weight coefficient of the p-th scattered path (constant for a given channel model).

The general input-output discrete-time channel model is expressed as([26])

$$y(t) = \sum_{p=0}^{P-1} a_p \mu_p(t) x(t - \tau_p), \tag{3.10}$$

where:

$y(t)$: channel output,
$x(t)$: channel input, the transmitted signal,
P: total number of scattered paths,
$\mu_p(t)$: fading behavior of pth path, which is a complex Gaussian process.

From (3.10), it is inferred that the output of the fading channel can be regarded as a weighted superposition of P paths, multiplied by a weight factor a_p and a time varying phase function $\mu_p(t)$, which is responsible for the phase rotation of the received signal, $y(t)$.

In the following sections, the aeronautical channel models are classified according to the experienced flying scenarios [27].

3.2.1 En-route

In En-Route (ENR) channel scenario, the AC is assumed to be cruising at an average speed of about 600 Knots True Airspeed (KTAS), which is equivalent to 308 m/s. The

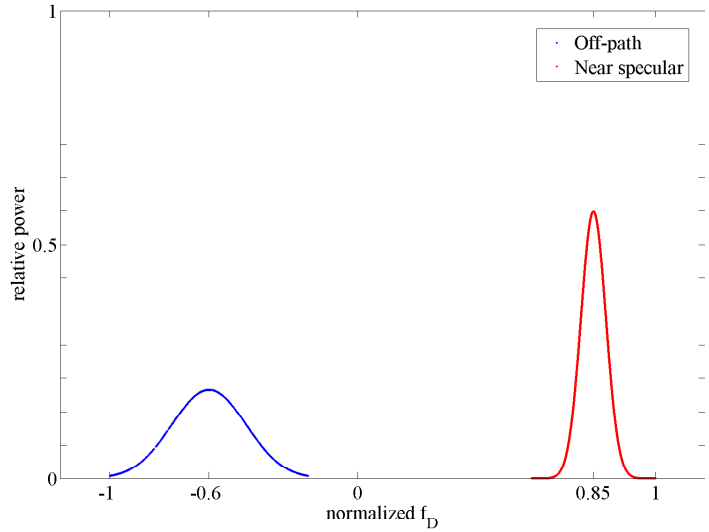

Figure 3.3: En-route Doppler power spectrum follows a Gaussian distribution.

cell size is 200 NM, corresponding to 370 km. The channel is modeled as a strong LOS component, a near specular echo, and a longer delayed off-path scatterer. The near specular echo occurs at $\tau = 0.3$ μs and the off-path echo occurs at $\tau = 15$ μs. When the GMSK modulated signal oversampled with a sampling rate F_s, the sampling period T_{OSR} is then larger than 0.3 μs. This implies that the near specular echo cannot be resolved within T_s and thus it is approximated to occur at $\tau = 0$ μs. Further, K_{Rice}, defined in (3.9), is equal to 15 dB.

At a speed of 600 Knots [26] with $f_c = 975$ MHz, f_{D} is 1 kHz. The Doppler power spectrum of the reflected paths follows a Gaussian distribution and can be seen in Figure 3.3. A summary of the ENR channel parameters is given in Table 3.1.

Table 3.1: ENR channel model parameters.

Parameter	Value
Maximum Doppler frequency	1000 Hz
Rician factor	15 dB
Near specular / off-path power ratio	6 dB
Mean Doppler of near specular echo	0.85 f_D
Mean Doppler of off-path echo	-0.6 f_D
Doppler spread of near specular echo	0.05 f_D
Doppler spread of off-path echo	0.15 f_D

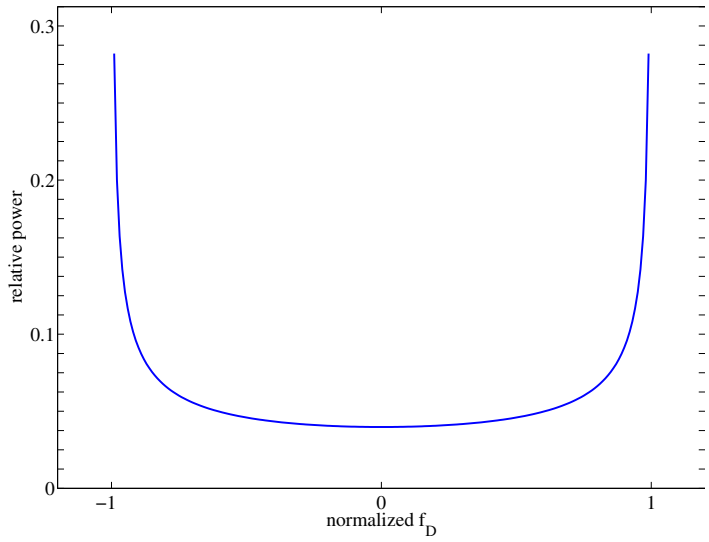

Figure 3.4: Take-off landing Doppler power spectrum, following a Jakes distribution.

3.2.2 Taking-off/Landing

This channel model, also known as Terminal Maneuvering Area (TMA), corresponds to the communication between the AC when it is taking-off or landing and the GS. The corresponding cell size of the TMA is 75 NM (which is equivalent to 139 km). A strong LOS component is again assumed but now due to the low altitude at which the AC is flying, strong scatterers are observed. When the AC is on the runway just before taking-off, considerable reflections and scatterers from adjacent buildings are observed.

On the extreme case, when the AC is just about to landing and flying at very low heights, there is again a LOS with many scatterers. The final model will be approximated by an exponential decaying power profile with $\tau_{\max} = 20\mu$s.

The maximum Doppler shift according to a TMA speed of 300 KTAS [26] (equivalent to 154 m/s) is 500 Hz. For the worst case scenario, when the scatterers from surrounding buildings are isotropically distributed, the Doppler power spectrum follows a Jakes distribution, as illustrated in Figure 3.4. A summary of the TMA channel parameters is given in Table 3.2.

Table 3.2: Take-off landing channel model parameters.

Parameter	Value
Maximum Doppler frequency	500 Hz
Rician factor	10 dB
Maximum access delay	10 μs

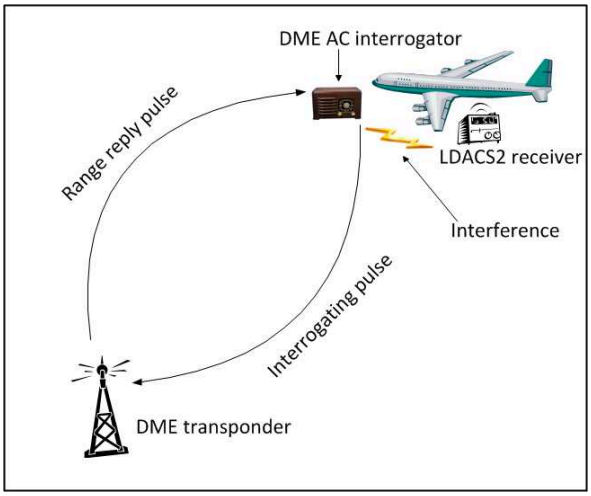

Figure 3.5: DME co-site interference.

3.3 Interference from Legacy Systems

In aeronautical communications, there exist many sources of interference that have to be taken into account. Referring to Figure 1.4, LDACS2 is supposed to be implemented adjacent to the legacy DMEs in the L-band. DME is an old, yet still used, navigation system that estimates the slant range distance (and the AC speed in some systems). The DME interrogator installed on-board the AC requests the transmission of a pulse pair from the DME transponder at the GS. Then, the DME GS transponder replies after a fixed delay and at fixed frequency offset of $f_c \pm 63$ MHz. By analyzing the Round Trip Time (RTT) of received pulses, the DME interrogator on-board of the AC can determine its distance from the DME GS, see Figure 3.5.

The typical DME transponder emits a peak pulse power of 1 kW, which is considerably high compared to the LDACS2 transmitter installed on-board the AC, with a maximum transmit power of 50 W. In LDACS2 GS, high power interference from adjacent DME GS can be avoided by the large separation of the LDACS2 GS antennas. On the other hand, when the AC is using both LDACS2 and DME interrogator, co-site interference arises. This co-site interference happens whenever the DME interroga-

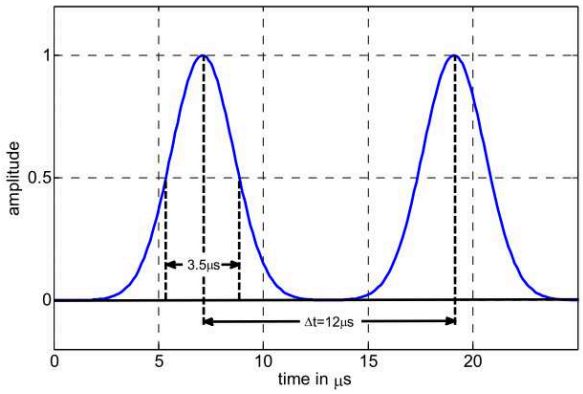

Figure 3.6: DME pulse pair in time domain [3].

tor transmits pulses on the same time that the LDACS2 receiver receives data from LDACS2 GS. This co-site interference cannot be avoided because of the insufficient separation between DME and LDACS2 antennas located on the same AC. The DME transmitted pulses $p(t)$ are Gaussian shaped, generated in a pairwise manner as [3]

$$p(t) = \exp\left(\frac{-\alpha t^2}{2}\right) + \exp\left(\frac{-\alpha(t-\Delta t)^2}{2}\right), \tag{3.11}$$

where:

α: the width of a single pulse (3.5 μs),
Δt: the spacing between the pulses, which is 12 μs in X mode and 30 μs in Y mode [30].

In the simulations, the duration of a single pulse is set to be exactly equal to T_b, i.e., 3.69 μs. This considers the best case scenario, in which the DME single pulse will fit exactly into one T_b. Considering a single pair of DME pulses in time domain, and taking into account the rise and decay time of 2.5 μs, the total disturbance duration of the DME signal is approximated to 17 μs, which equals 5 T_b, as shown in Figure 3.6.

4 LDACS2 Receiver

The GSM receiver can be adapted to LDACS2. However, many aspects have to be adapted to the LDACS2 slot structure. Due to the different frame structure, many aspects have to be adapted according to the LDACS2 structure. One of them is the location of the training sequence at the beginning of the LDACS2 burst while it is located in the middle of the GSM burst. This is a critical issue in channel estimation because the existence of the training sequence in the middle of the burst helps the receiver to correctly estimate the channel. Moreover, the length of the GSM burst is shorter than that of LDACS2 burst. Therefore the estimated channel in GSM is valid for the total GSM burst duration while the LDACS2 estimated channel is only valid for a part of the burst. As a result, more efficient channel equalization and coding techniques are needed in LDACS2 to cope with the extended burst length.

The main contribution of this chapter is the implementation of the LDACS2 receiver according to the specifications. The parts of the LDACS2 receiver are described along with their implementation techniques. The effective channel equalization to cope with high Doppler spreads experienced in aeronautical communications is also implemented. Moreover, channel coding schemes are needed to mitigate the channel effects. This chapter also describes the coding schemes parameters which are implemented in the LDACS2 receiver simulator.

The chapter begins with a description of the GMSK demodulator. The different parts of the demodulator are discussed. The implementation issues are introduced. Then, the techniques to mitigate the channel effects are considered.

4.1 GMSK Demodulation

Since GMSK is basically a phase modulation technique [15], the information is carried in the phase of the signal. Thus, analyzing the phase is essential to determine the

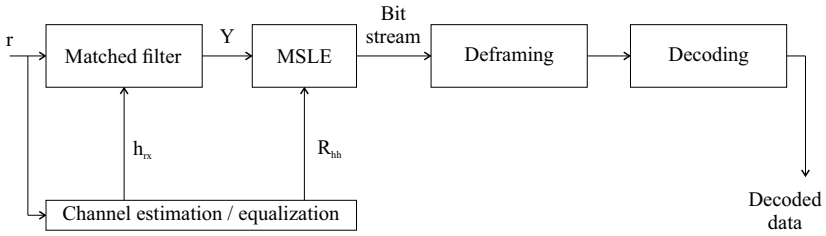

Figure 4.1: LDACS2 receiver architecture.

originally transmitted signal. Since the Gaussian filter introduces ISI in the transmitted signal to reduce transmission bandwidth, recovering the original data is a non-trivial task. Data recovery requires using an efficient algorithm to determine what sequence of data was most likely sent. The most widely used algorithm is the MLSE algorithm.

A typical GMSK receiver is shown in Figure 4.1. The received signal r is filtered by a matched filter. The matched filter uses the information from the channel estimator to adapt the filter impulse response accordingly. The output from the matched Y is fed to the MLSE block. The MLSE outputs a bit stream containing the encoded user data plus redundancy bits. The demultiplexer removes the header, trailer and other redundant bits from the demodulated bit stream and extracts the encoded bits. Then, the channel decoder recovers the data bits against transmission errors.

The matched filtering and channel estimation are done alongside with each other because the matched filter uses the oversampled received sequence and the knowledge of the channel taken from channel estimator to produce a down-sampled data sequence to the next stage, the MLSE algorithm. In turn, the channel estimator predicts the channel impulse response based on a 26-bit training sequence used at the beginning of each burst.

Referring to (2.13) and using the discrete time notation, the Gaussian filter impulse $g[n]$ is expressed as

$$\acute{g}[n] = g\left[n - \frac{L}{2}\right] w_l[n], \tag{4.1}$$

then the transmitted baseband signal $x[n]$ is written as [16]

$$x[n] = \sum_i a_i \acute{g}[n-i] \tag{4.2}$$

where a_i is the differentially encoded transmitted binary bits.

At the receiver, the effective channel impulse response $h_{rx}[n]$ is the convolution of the transmitter Gaussian filter $\acute{g}[n]$ and the channel impulse response $h_c[n]$ and is expressed as

$$h_{rx}[n] = \acute{g}[n] * h_c[n]. \tag{4.3}$$

Then the received baseband signal $r[n]$ can be written as

$$r[n] = \sum_{l=0}^{L-1} a_l h_{rx}[n-l] + \eta[n], \tag{4.4}$$

where $\eta[n]$ is the AWGN with variance N_0 and L is the number of channel taps.

The matched filter at the receiver has an impulse response $h_m[n]$, expressed as

$$h_m[n] = h_{rx}^*[n], \tag{4.5}$$

where $h_{rx}^*[n]$ is the time reversed complex conjugate of the effective channel impulse response function, $h_{rx}[n]$.

As in GSM, LDACS2 uses a predefined pilot sequence, called Training Sequence (T_{seq}), to estimate the effective transmission channel impulse response. The used T_{seq}, which is one of eight training sequences defined for GSM, has to be known to both the transmitter and the receiver. In order for the channel estimator to correctly approximate

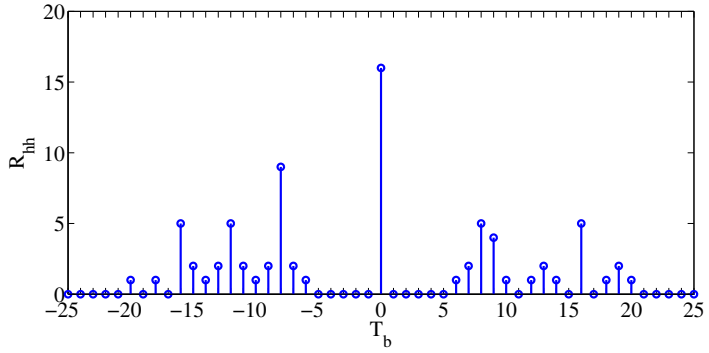

Figure 4.2: Auto correlation function characteristics of the training sequence.

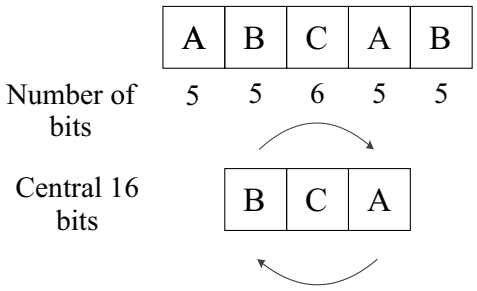

Figure 4.3: Cyclic structure of the training sequence.

the channel response, T_{seq} should have an impulse-like autocorrelation function and L zeros around, as shown in Figure 4.2.

Although T_{seq} consists of 26 bits, only the central 16 bits are used for channel estimation. This is because of the cyclic structure 'ABCAB' of the T_{seq} [17], as seen in Figure 4.3. In other words, to ensure the estimated channel autocorrelation function R_{hh} to be cyclic, part A and part B are added at the start and the end of the burst, respectively. The length of 5 bits of each A and B parts ensures the existence of five zeros on both sides of R_{hh}.

4.1.1 Channel Estimation

When the training sequence T_{seq} is sent over the channel, the received training sequence $r_{T_{\text{seq}}}$ is described as

$$r_{T_{\text{seq}}} = T_{\text{seq}} * h_{rx}[n] + \eta[n]. \tag{4.6}$$

Since the receiver has full knowledge of the transmitted T_{seq} as well as its exact position (assuming perfect synchronization), R_{hh} is found by convolving the complex conjugate of the 16 middle bits of the received training sequence $r_{T_{\text{seqc}}}$ with the locally generated version of T_{seqc}.

The operation is described mathematically as

$$\begin{aligned} R_{hh} = r_{T_{\text{seqc}}} * T^*_{\text{seqc}} &= T_{\text{seq}} * T^*_{\text{seqc}} * h_{rx}[n] + \eta[n] * T^*_{\text{seqc}} \\ &= \begin{cases} R_{hh}[0]h_{rx}[n] + \eta[n] * T^*_{\text{seqc}}, & \text{for} \quad n = 0, \\ \eta[n] * T^*_{\text{seqc}}, & \text{for} \quad n = \pm1, \pm2, \pm3, \pm4, \pm5, \end{cases} \end{aligned} \tag{4.7}$$

where T_{seqc} are the central 16 bits of T_{seq}.

Comparing the term $R_{hh}[0]h_{rx}[n]$ with the second term $\eta[n] * T^*_{\text{seqc}}$, the first term is obviously larger than the second. This is due to the factor of $R_{hh}[0] = 16$ as illustrated in Figure 4.2. For $n \neq 0$, the term $\eta[n] * T^*_{\text{seqc}}$ is relatively small compared to $R_{hh}[0]h_{rx}[n]$. Thus, (4.7) is approximated to

$$\begin{aligned} R_{hh} &\approx T_{\text{seq}} * T^*_{\text{seqc}} * h_{rx}[n] \\ &\approx \begin{cases} 16h_{rx}[n], & \text{for} \quad n = 0, \\ 0, & \text{for} \quad n = \pm1, \pm2, \pm3, \pm4, \pm5. \end{cases} \end{aligned} \tag{4.8}$$

It should be noticed that the noise term $\eta[n] * T^*_{\text{seqc}}$ is no more AWGN, rather colored noise. The coloration comes from the phase rotation of the original transmitted signal plus the introduced ISI of the filter. This approximation does not affect the performance, since the channel estimator is capable of estimating the channel when the Signal-to-Noise Ratio per Bit E_b/N_0 is reasonably sufficient.

Examining (4.8), the effect of choosing a good T_{seq} is obvious. That is, a channel with a maximum length of $L - 1$ bits duration can be estimated with high accuracy, with L being number of zeros surrounding the center peak of R_{hh}. Due to the best known

training sequences, a maximum channel length of $L_h = L - 1$ taps can be estimated. Each tap corresponds to 1 bit duration, which is 3.69 μs in LDACS2.

To determine the starting of the burst as well as the channel estimation, the sliding window approach is used [10]. This is done by squaring R_{hh}, obtained from (4.8), to have the energy signal $e[n]$, expressed as

$$e[n] = |R_{hh}|^2. \tag{4.9}$$

$e[n]$ is then searched for the maximum peak to obtain the first sample of the channel impulse. The m highest energy samples are found using the search window technique we$[m]$ according to

$$\text{we}[m] = \sum_{k=m}^{m+L} e[k]. \tag{4.10}$$

Having found m samples within the window length L, the maximum we$[m]$ value represents the beginning of the actual channel response, $h_{rx}[1]$. The samples contained in we$[m]$ represent the best estimation of the total channel. The estimated downsampled channel impulse response $\hat{h}_{rx}[n]$ is calculated as [18]

$$\hat{h}_{rx}[n] = \frac{v[k + nF_s]}{16}, \tag{4.11}$$

where k is the first sample in we$[m]$.

Besides, R_{hh} is used as an input to the channel equalizer described in Section 4.1.3.

4.1.2 Matched Filter

Having estimated the channel, the matched filtering is expressed as the inner product of every N samples of $r[n]$ with $\hat{h}_{rx}[n]$, where N is the number of samples in $\hat{h}_{rx}[n]$. The operation is mathematically described as

$$Y[m] = \sum_{n=1}^{N-1} r[n + mF_s]\hat{h}_{rx}[n], \tag{4.12}$$

The output of the matched filter Y is passed to the channel equalizer. The MLSE detector is used to estimate the most likely transmitted sequence. Section 4.1.3 describes the function of this estimator.

4.1.3 Maximum Likelihood Sequence Estimator (MSLE)

Due to the introduced ISI in the transmitted sequence of data, the modulation of the transmitted data is a nonlinear operation. Hence, the estimation of the originally transmitted sequence becomes a non-trivial task. Among many receivers for the GSM system, the MLSE based on Viterbi algorithm is the most popular and efficient one, which was originally proposed by Forney [19]. The MLSE detector is the second block of Figure 4.1.

It is known that the GMSK modulation has a memory structure. That is, the symbol estimation at time t is highly correlated to the symbols preceding in time. This correlation is caused by the Gaussian filter and the channel effect. Furthermore, only a certain number of symbols in the past are needed to be considered, since there are only few legal states that need to be considered for the optimization process. This is very similar to the decoding of symbols encoded by a convolutional coder. The decoding process of the sequence could be very complex if implemented using the probabilities technique. Fortunately, using the Viterbi algorithm, the complex task reduces to a problem of dynamic programming. In the LDACS2, similarly to the GSM, the maximum length of the estimated channel impulse response $\hat{h}_{rx_n}$ has a length of $4T_b$. This is to reduce the complexity of the receiver and to cope with high data rates. Given

that the GMSK constellation size is 2, the number of possible states M at any time that the MLSE equalizer would have is

$$M = 2^{L_h+1}, \tag{4.13}$$

where L_h is the number of estimated channel taps. As a result, the estimated symbols constitute a finite state machine, with each MSK symbol uniquely determined by the previous $L_h - 1$ symbols. This state machine is known as the trellis structure, with each state at time $[m]$ expressed as:

$$\sigma[m] = I[m], I[m-1], ..., I[m-(L_h-1)]. \tag{4.14}$$

Since a GMSK symbol can only take one of the four values $\{1, -1, j, -j\}$ at time m, (4.14) shows that for a certain state $\sigma[m]$, the symbol $I[m]$ is uniquely determined by the $L_h - 1$ symbols before. . Furthermore, considering the alternating state diagram of MSK in Figure 4.4, if a symbol at time m is real {1 or -1} then the symbol at time $m + 1$ is complex {j or -j}. At the end of each symbol interval, the GMSK symbol is found to be

$$\alpha[m] = \begin{cases} \pm 1, & \text{for } m \quad \text{odd}, \\ \pm j, & \text{for } m \quad \text{even}. \end{cases} \tag{4.15}$$

Therefore, the number of legal trellis states at any given time is reduced by a factor of 2, implying the total number of states at time m to be $M/2$. Referring to Figure 4.4, the total number of states is reduced to 4 in this example. Another observation indicates that any state has only two legal next states, which also implies that any state has only two legal previous states.

To give a better understanding of MSLE equalizer, the Viterbi algorithm is explained in short in Section 4.1.4.

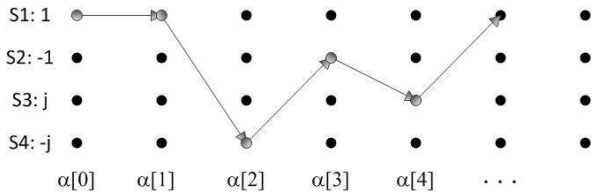

Figure 4.4: Trellis structure example for $L = 2$ and 2^L states.

4.1.4 The Viterbi Algorithm in the LDACS2 Receiver

For a given system there is a limited number of valid states M [21] and the resulting phase states $\theta[m]$ are expressed as

$$\theta[m] \in \{0, \frac{2\pi}{p}, \frac{4\pi}{p}, ... \frac{(p-1)2\pi}{p}\} \tag{4.16}$$

In GMSK, the possible phase states are limited to 0, $\pi/2$, π and $3\pi/2$. Therefore the paths along the trellis merge into a certain number of states after a certain period in time. Knowing this fact and the number of time samples that affect the path selection, a considerable complexity reduction is achieved. The Viterbi algorithm selects and updates $2^{M/2}$ surviving sequences and store them in the memory at each time instant n. At the end of the decoded sequence, the MLSE detector selects the survivor path with the minimum Hamming distance. The Viterbi Algorithm is summarized into the following steps [21]:

1. **Branch Metric Calculation**
   For a given number of states, M, there are 2^M next states, from which the Viterbi algorithm has to calculate the one with the best metric. Referring to the discussion in 4.1.3, the valid next or previous states are limited to $M/2$. For a given received sequence, there is single path in the trellis. Each path consists of a chain of branches and each branch is associated with a symbol in the trellis. The branch metric is calculated as the correlation between the output of the matched filter $Y[n]$ and the possibly originally transmitted MSK symbols $a[n]$. The autocorrelation function of the estimated channel impulse response, R_{hh}, is provided by the channel estimator.

The branch metric γ calculation is expressed as [10]

$$\gamma[n] = a^*[n]R_{hh}(0)a[n] + 2\Re\{a^*[n] \sum_{m=n-L_h}^{n-1} a[m]R_{hh}[n-m]\}. \tag{4.17}$$

Since $a^*[n]a[n] = 1$, the first term in (4.17) is fixed for all the branches and can be omitted. Then (4.17) is simplified to

$$\gamma[n] = 2\Re\{a^*[n] \sum_{m=n-L_h}^{n-1} a[m]R_{hh}[n-m]\}. \tag{4.18}$$

2. **Path Metric Calculation**

   According to Ungerboeck's recursive form [20], the path metric ψ is calculated as

$$\psi(Y[n]) = \Re\{a^*[n]Y[n]\} - \gamma[n]. \tag{4.19}$$

3. **Path Update**

   Since there are r possible branches leaving each state at time n, the selection of the survival path is done by finding the path that maximizes (4.19). The number of survival paths at the end of information sequence is equal to L.

4. **Path Decision**

   The final step is simply choosing the path, among M, that has the maximum path metric ψ. In case that hard-decision is implemented, the output of the Viterbi Equalizer is $\hat{a}[n]$, which is the sequence of symbols a long the selected trellis path.

$\hat{a}[n]$ is in the form of Non-Return-to-Zero (NRZ), is directly converted to RTZ bits. Then the originally transmitted symbols $\hat{x}[n]$ are retrieved as

$$\hat{x}[n] = \frac{\hat{a}[n]}{j\hat{x}[n-1]\hat{a}[n-1]}. \tag{4.20}$$

In case that soft-decision decoding is implemented, the output of the Viterbi algorithm is not hard-limited to ± 1, but rather quantized. It is found [21] that a quantization level of 8 introduces a gain of about 2 dB in Eb/No compared to hard-quantization. For instance, a Viterbi output level of +4 indicates high confidence that the transmitted bit was 1 whereas +1 indicates less confidence. For benefit, the soft-decision Viterbi output should be fed to the input of a soft-convolutional decoder.

An important characteristic of GMSK Viterbi Equalizer is that a single error will never occur (see discussion 6.2.7,[21]). That is, either double or burst bit errors will occur. That is because even in the case of a single bit error, the survivor path will never converge with the error-free path. This feature is exploited by converting double errors into single errors, which is done by the differential encoding and decoding, at the transmitter and receiver, respectively.

4.2 Mitigating Fading Channel Effects

When the ACs are overflying, maneuvering or taking off in rather crowded airports, the experienced channel models are far from being pure AWGN (as described in Chapter 3). This section describes the techniques used to mitigate the fading channel effects. Those techniques include channel coding and interleaving. For the sake of consistency, they are discussed in the same context. Referring to Figure 4.5, one easily notices the fading effect on the error performance of a communication system. In the case of an AWGN channel (ideal channel), the effect of noise could be easily mitigated by only increasing the Signal-to-Noise Ratio (SNR). On the other hand, for flat fading channels within Rayleigh limit, i.e., no LOS components, the performance of the system degrades severely. However, the bad performance of the system could be enhanced by

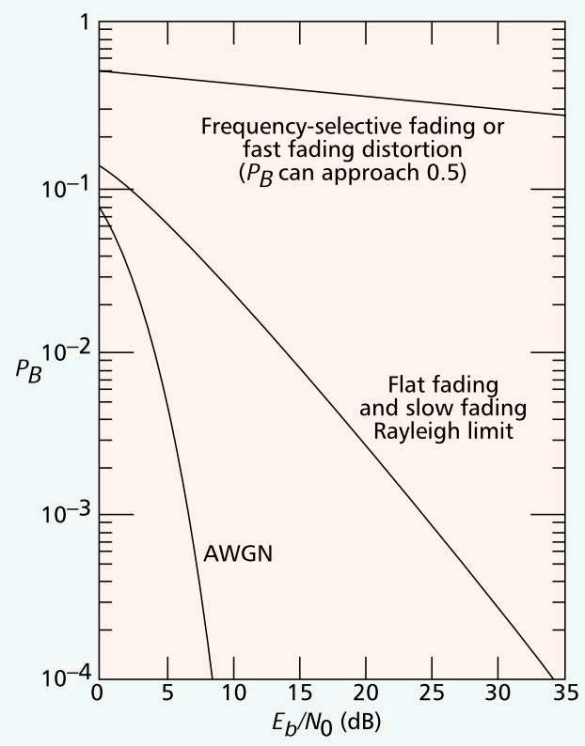

Figure 4.5: The good, the bad and the awful error performance [22].

increasing the SNR [22], even though this would be no feasible solution to increase it beyond practical SNR values.

On the extreme case, which is though very common in Aeronautical Communication, the frequency-selective fading or fast fading (ENR or TMA channel models) introduces irreducible error rate performance. No matter how much the SNR is increased, the error floor remains at high level and no possible communication could be established. Fortunately, the performance can be enhanced using channel equalization techniques. The MLSE equalizer described in 4.1.3 is a well known technique. By using the appropriate coding type, error-floored BER curve could further be enhanced. The BER after coding approaches the same AWGN performance for high efficiency codes. In the next section a brief description of the FEC techniques is introduced.

4.2.1 Forward Error Correction

In wireless communication channels, FEC is an important part of the system, because with a wise choice of the encoder at the transmitter side, the receiver is able to correctly

recover the transmitted data, even if errors have occurred. Generally, there are two kinds of errors [22] occurring in the transmitted data:

1. Random errors: they tend to occur because of the thermal noise existing at the front end of the receiver (generally approximated as AWGN).

2. Burst Errors: the errors in this case occur in a burst fashion (subsequent groups of symbols are corrupted) due to the fading channel effects. Due to their dependency, burst errors are said to have memory. This memory is equal to the the fading channel length, L_h [23].

The random errors are efficiently mitigated by using some popular FEC codes. Convolutional codes with maximum correcting capabilities [24] are mostly used to mitigate random errors. Those codes are capable of correcting transmission errors, given that the error pattern would not exceed the correcting capability of the coder, t. Where t is defined as

$$t = \frac{d_{\min} - 1}{2} \tag{4.21}$$

Where $d_{\min}$ is defined as the smallest number of places (in bits) that any two code words differ in the codebook. Obviously, codes with large $d_{\min}$ are a good choice. Unfortunately, increasing the minimum distance also decreases the code rate R_c which is defined as

$$R_c = \frac{k}{n}. \tag{4.22}$$

Where k is the message length and n is the code word length. The other type of coders are the block codes, which operate on a block basis rather than a bit basis. One of the most popular coders is the Reed Solomon (RS) coder, which is a non binary cyclic coder based on Galois Field (GF) area of mathematics. The notation RS(n, k, m) is often used, where n is the total number of symbols in the encoded block, k is the number of encoded data symbols and m is the symbol length, in bits. Taking RS$(15, 11, 4)$ as an example, this code can correct up to 2 symbols errors, each symbol of 4 bits. That

means a burst error of 8 bits can be corrected, given the error is exactly limited to 2 symbols.

It is always desirable to reduce the redundant bits as much as possible, i.e., increasing the system throughput. Hence, there is a trade off between increasing code rate and the number of errors that a coder can correct. Besides, decreasing R_c below a certain limit will degrade the performance of the system, as seen in Figure 4.6 [25]. This figure implies that the optimum RS code rate for a Gaussian channel is around 0.6. On the other hand, for a Rician channel the optimal RS code rate is ranging from 0.4 to 0.6. The reason for the degradation of the BER performance at high R_c is, that the less coding is applied to information bits, the more errors will occur.

The degradation at low R_c is more severe than that at high R_c. Two opposite mechanisms at low R_c are observed: the first one is the increased coding redundancy, which tries to mitigate errors. The second mechanism is the reduced energy per modulation symbol (compared to the information bit energy), which results in more errors in the demodulator. Finally, the second mechanism wins and thus the system error-performance degrades.

Some techniques are used, however, to enhance the coders correction capability, keeping R_c as high as possible, such as puncturing used in convolutional coding. However, R_c cannot exceed a certain upper limit, as previously discussed.

To achieve a better performance in LDACS2, concatenated coding is considered, as seen in Figure 4.7. With the suitable choice of coding parameters, concatenated codes can achieve very high coding gains with efficient coding. The idea is simple: the outer coder (usually a block coder) is responsible for correcting burst errors that occurring from the convolutional coder while the inner coder (usually a convolutional coder) corrects random errors. The random errors are non-correlated and related to the AWGN.

The LDACS2 coding parameters are listed in Table 4.1.

4.2.2 Interleaving

Another useful technique is to use interleaving together with channel coding. The interleaver function is simply spreading the bits (groups or individuals) within the transmitted frame, after the coding block. The result is that correlated errors are

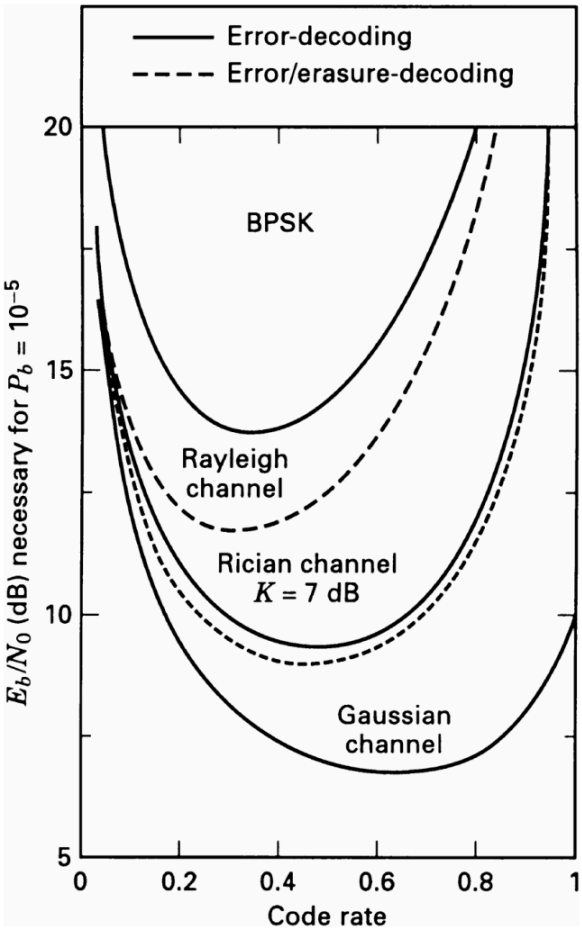

Figure 4.6: RS BER vs. code rate trade-off [25].

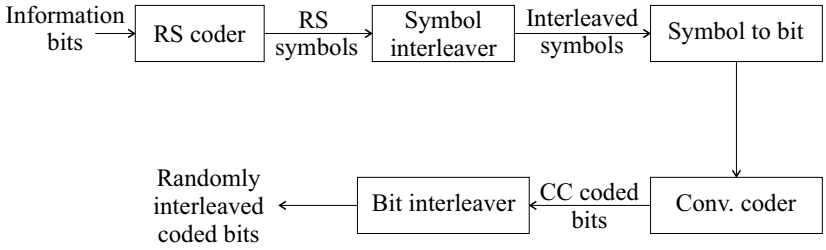

Figure 4.7: Concatenated channel coding for LDACS2.

distributed among several code words, which leads to less errors per single code word. This helps the coder to successfully correct the errors within its capability. There are several types of interleavers described in the literature [24]. The Block interleaver, recommended for LDACS2, makes the channel with memory L behave like a random channel to the decoder. This results in less powerful codes are required to correct transmission errors. At the transmitter, the block interleaver takes a block of bits and writes them row-by-row fashion into a matrix and then reads the matrix into a

Table 4.1: LDACS2 coding parameters.

Parameter	Value
Inner coder	convolutional $(7, 171, 133)$
Puncturing pattern	[110101] for $R_c = 3/4$
Bit interleaver	quasi random
Outer coder	RS$(15, 11, 4)$ or RS$(31, 23, 5)$
Outer interleaver	symbol interleaver
Coded BER	10^{-7} for uncoded BER of 10^{-3}

column-wise fashion to feed the modulator. At the receiver, the operation is reversed. The filling and reading the matrix introduces delays in the transmission chain.

The bit interleaver, on the other hand, is used after the convolutional coder to decorrelate the AWGN effect and to randomize the bits within LDACS2 slot. The bit interleaver, however, is simpler and there is no buffering delay introduced.

The use of both types of interleavers as well as the coders is intensively analyzed within the LDACS2 against different aeronautical fading channels in Chapter 5.

5 LDACS2 Performance and Capacity

As stated in Chapter 1, the performance evaluation of LDACS2 is important in the selection of the final LDACS proposal. In addition to AWGN, the system has to be tested against the two main flying scenarios, those are the ENR and TMA channel models.

In this chapter, the LDACS2 simulator is described in short. The simulation parameters are given. The system is then tested against the AWGN channel. Next, the specified coding schemes are applied to the LDACS2 under the AGWN as well as ENR and TMA channel models. More efficient code rates are proposed and tested under the same conditions as well. The performance of the system is evaluated using the BER as measure. The co-site interference from the DME interrogators is also studied. Then, the system performance against time synchronization and frequency estimation errors is investigated. Later, the system capacity is studied within the suggested specifications. Finally, the LDACS2 performance is compared to the LDACS1 within the specified coding parameters.

5.1 LDACS2 Performance under Aeronautical Channel Models

In this section, the LDACS2 simulator is described. However,the main transmitter and receiver functions are described in detail in the Chapters 2 and 4 respectively.

5.1.1 LDACS2 Simulator

The LDACS2 simulator is built using the MATLAB simulation environment. The MATLAB communications system toolbox is used. The outer coder, the symbol in-

terleaver, the inner coder, and the bit interleaver are built according to the LDACS2 specifications. The modulator and demodulator parts described in Chapters 2 and 4, respectively, are partly adapted from the GSM simulator presented in the work [10]. However, the function implementation of the matched filter and the Viterbi algorithm have been redefined according to the LDACS2 specifications to yield soft output. The matched filter in LDACS2 should track the training sequence at the start of each burst, taking into account the guard bits added and the message addresses, which is the main difference from the GSM burst. The matched filter has also been redesigned to take advantage of the oversampled samples in the time domain for better channel estimation. The aeronautical channel models are implemented in Java [27] programming language and integrated into the MATLAB channel simulator code.

The framing structure of LDACS2 is analyzed and implemented for different slot lengths, as seen in Section 1.3.3. The LDACS2 performance is tested first for the specified specifications. Then, the specifications were modified and the performance is tested again under the same channel models. Those adaptations include using stronger codes, insertion of extra training sequences and longer burst structure. One of the challenging tasks was to modify the matched filter according to the number of training sequence.

The simulations are done using the Monte Carlo simulation method. The SNR is simulated in the range from 0 to 16 dB. For each value of SNR, $2 \cdot 10^7$ random information bits are generated. This number of bits ensures a BER values of $1 \cdot 10^{-6}$ to be obtained.

In each iteration, the BER ratio is calculated according to

$$\mathrm{BER} = \frac{N_e}{N_T}, \tag{5.1}$$

where N_e is the number of information bits decoded incorrectly, and N_T is the total number of information bits.

5.1.2 LDACS2 Performance in AWGN

As stated in Chapter 1, LDACS2 has different slot types. The main difference among them is the length of each slot. This has an influence on the estimated channel impulse

response as well as the encoding-decoding implementation. In this section, the performance of LDACS2 in the AWGN channel is simulated and compared to the theoretical GMSK performance. Then, stronger codes are proposed and simulated.

The AWGN is a zero-mean complex Gaussian process, with a variance of σ_N^2 of the entire process. The AWGN is generated in the simulator according to

$$\sigma_N^2 = \frac{F_s}{2}\frac{1}{\mathrm{SNR}_l}, \tag{5.2}$$

where F_s is the sampling rate, SNR_l is the linear SNR, defined as

$$\mathrm{SNR}_l = 10^{\left(\frac{\mathrm{SNR}}{10}\right)}. \tag{5.3}$$

The generated noise is then added to the original transmitted signal samples $r[n]$ as

$$r[n] = x[n] + \sigma_N \cdot z[n], \tag{5.4}$$

where z is a function that generates normally distributed random values with a zero mean and a variance of one.

To test the LDACS2 receiver, the estimated channel impulse response $\hat{h}_{rx}$ is plotted and compared to the Gaussian pulse shape at the transmitter 2.6. Figure 5.1 shows that the estimated channel impulse response is approximately equivalent to the transmitter pulse shaping function. However, is it slightly broadened due to the AWGN. This means that the LDACS2 receiver can successfully estimate the channel impulse response.

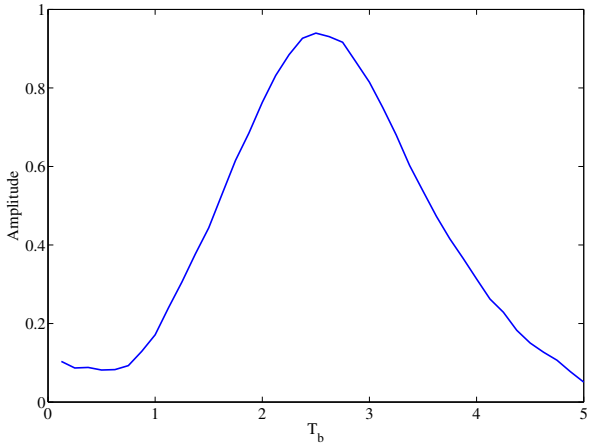

Figure 5.1: Estimated channel impulse response at the channel estimator.

For the LDACS2 Down Link (DL), the CoS1 uncoded AWGN performance is simulated and compared to the theoretical GMSK BER. The theoretical BER P can be calculated by [32]

$$P = \text{erfc}\left(\sqrt{\beta \cdot E_b/N_0}\right), \tag{5.5}$$

where:

β: is a factor related to BT product. For $BT = 0.3$, β is 0.89,
E_b/N_0 is the energy per bit.

Figure 5.2 shows that the LDACS2 uncoded BER performance is close to the theoretical GMSK BER performance. However, the theoretical BER does not consider the transmission channel impulse response, while the simulated BER assumes the existence of the transmission channel and estimates the channel impulse response $\hat{h}_{rx}$ accordingly (as defined Section 4.1.1). Hence the degradation in the simulated BER in comparison to the theoretical BER. On the other hand, the simulated BER matches the LDACS2 specifications [2].

Next, the specifications coding is simulated in the AGWN channel. In the practical implementation of LDACS2, the data bits are encoded. With coding, the information bit rate R_i is inversely proportional to R_c. Referring to the CoS1 slot structure in Figure 1.9, the information part is 144 bits and the FEC part is only 49 bits. Besides,

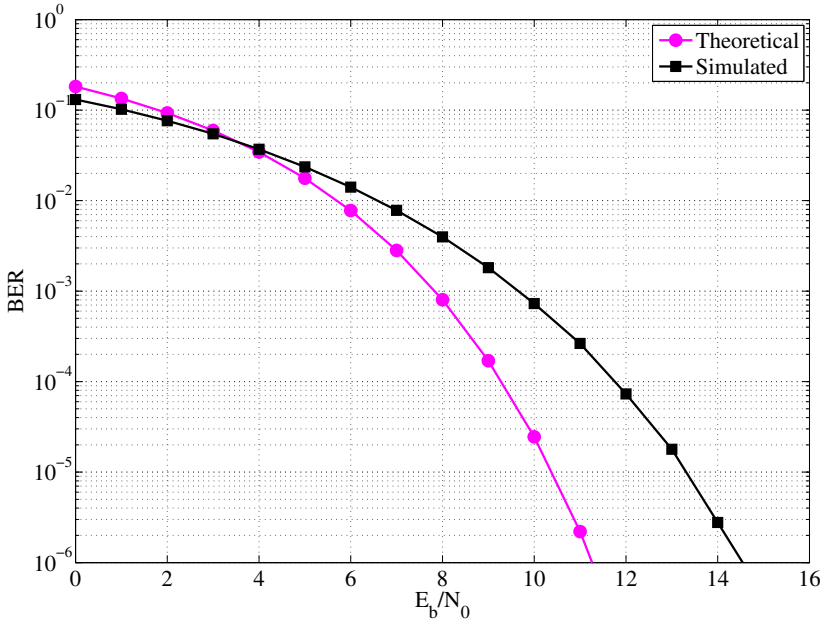

Figure 5.2: CoS1: non-coded AWGN.

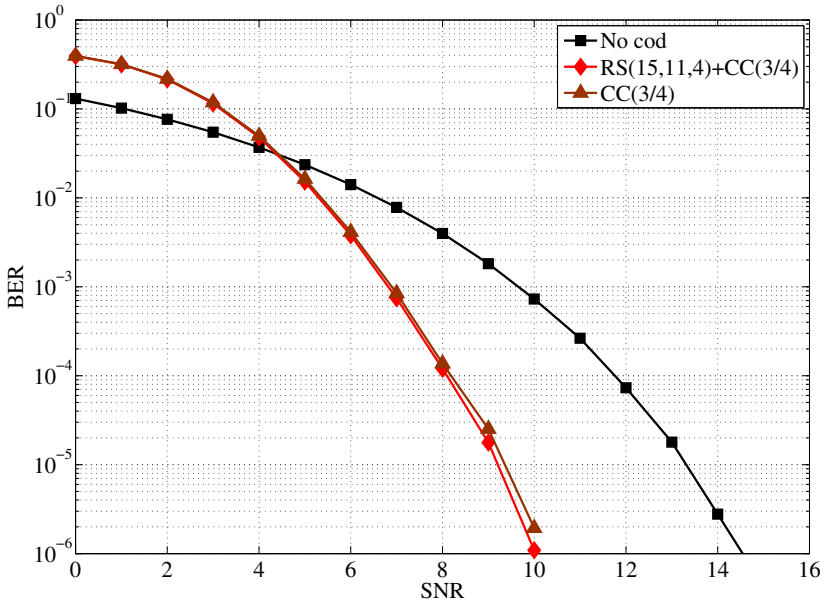

Figure 5.3: CoS1: coded AWGN, specifications coding.

only short code words, that can fit in the 193 bit-duration, can be used. Therefore, only RS code with $(15, 11, 4)$ concatenated with CC of $L = 7$ are considered.

Figure 5.3 shows the performance of both concatenated coding and single code. It is obvious that when using concatenated coding, no performance improvement is achieved. This is because the RS$(15, 11, 4)$ introduces no further enhancement on the

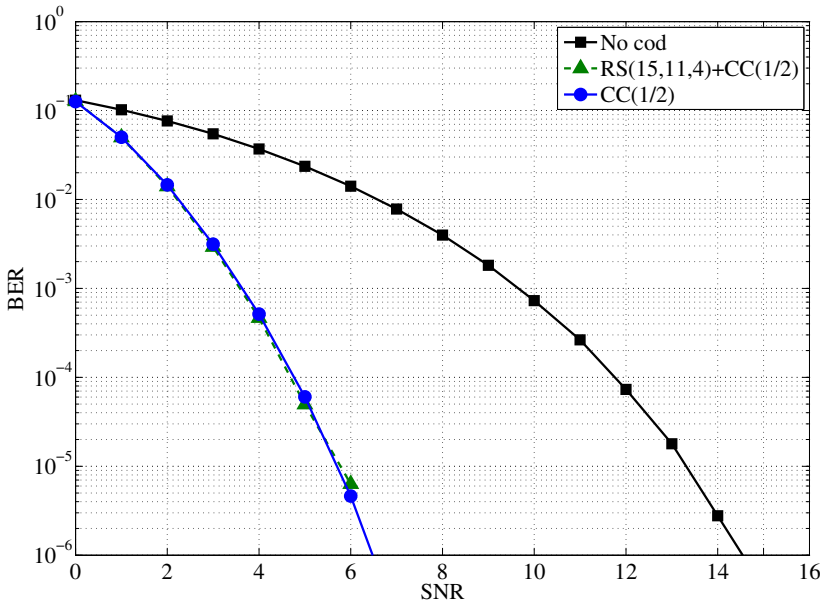

Figure 5.4: CoS1: coded AWGN (proposed coding).

error correction, since the slot length is short. This performance does not comply with the LDACS2 specification, which require a coded BER of 10^{-7} for an uncoded BER of 10^{-3}. Therefore, stronger coding is proposed. By using the same RS$(15, 11, 4)$ but with CC(1/2), the curves shown in Figure 5.4 are obtained. There is a gain in the performance of about 4 dB compared to CC(3/4). Again, a CC with ($R_c = 1/2$) performs the same as the concatenated coding.

The CoS2 slot performance in the coded AWGN using the specification coding is considered next. The CoS2 slot length is 1806 bits, which is equivalent to 6.66 ms. The user data part is 1304 bits and the FEC part is 394 bits (see Figure 1.10). The performance of CoS2 in the coded AWGN channel using the recommendation coding is shown in Figure 5.5. Since the CoS2 slot is longer than CoS1, longer code is used. Hence, RS$(31, 23, 5)$ concatenated with CC(3/4) are used. It can bee seen that the performance of concatenated coding for the CoS2 slot is better than a CC(3/4).

It is also possible to have a CoS2 burst, containing longer messages and spanning multiple CoS2 slots (as mentioned in Chapter 1). The AWGN performance of a CoS2 burst spanning 10 CoS2 slots is shown in Figure 5.6. Compared to a single slot, the BER of a CoS2 burst has a performance gain of about 2 dB using the same coding. This is due to the fact that the RS symbol interleaver can spread adjacent symbols over multiple RS codewords and thus less errors occur per single RS code word.

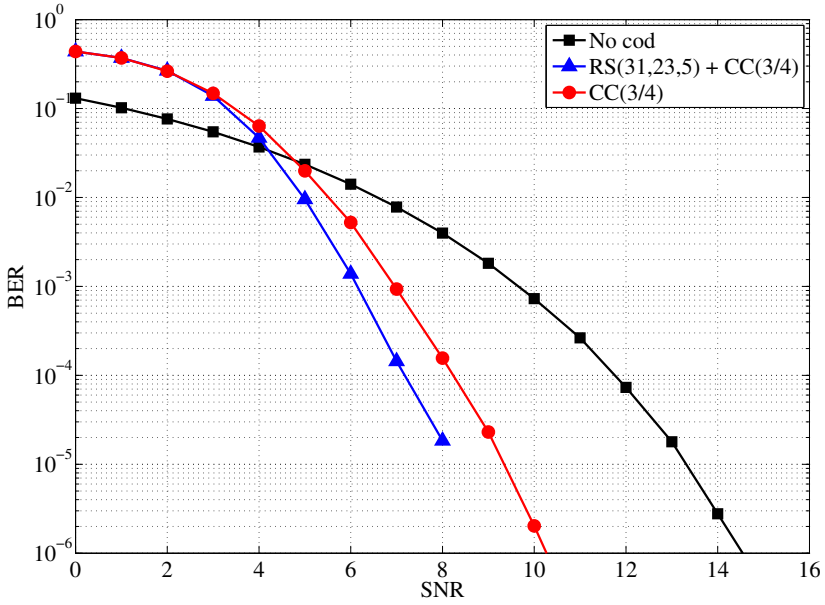

Figure 5.5: CoS2 slot: coded AWGN (specifications coding).

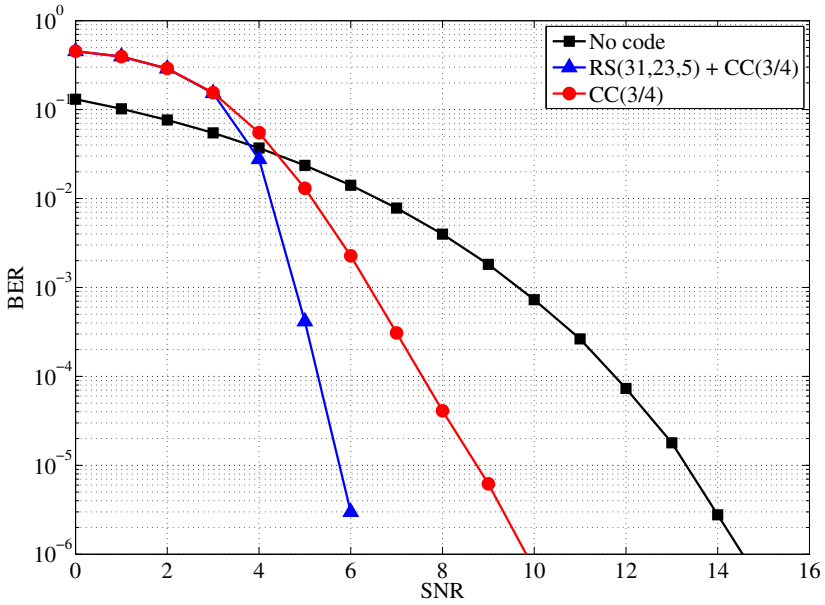

Figure 5.6: CoS2 burst: coded AWGN (specifications coding).

The LDACS2 Up Link (UL) performance is shown in Figure 5.7 for a UP burst of length 13.3 ms. From this figure, it can be inferred that the performance of a UP burst is similar to that of a CoS2 single slot.

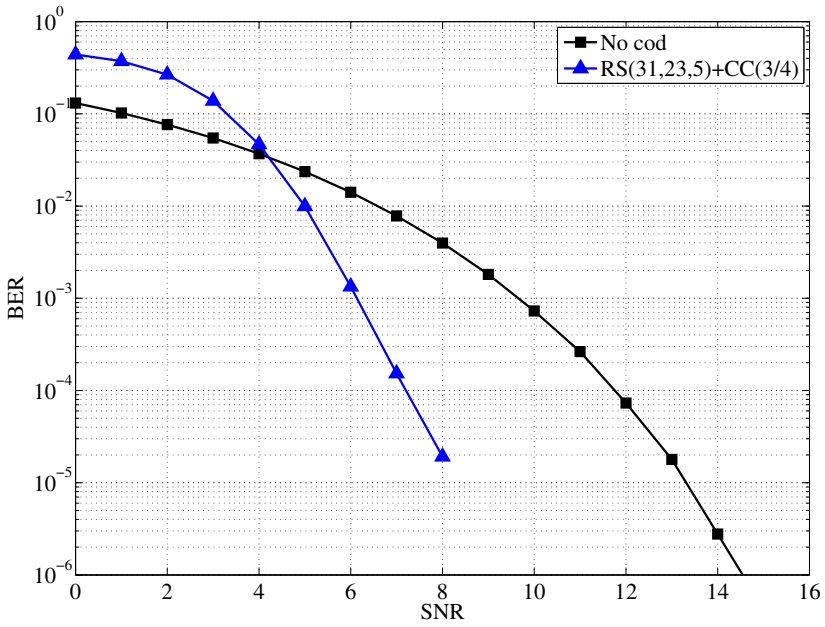

Figure 5.7: UP burst: coded AWGN (specifications coding).

It should be mentioned that the BER performance for the CoS2 slot, burst and UP burst can also be enhanced by using CC(1/2) concatenated with RS$(31, 23, 5)$, as shown in Figure 5.4.

5.1.3 LDACS2 Performance in ENR Channel

In this section, the LDACS2 performance in the ENR channel model is simulated. As mentioned in Chapter 3, the ENR channel model has two taps, the first is the LOS echo while the other is the off-path echo. The ENR channel power delay profile is shown in Figure 5.8.

For the simulations, perfect time and frequency synchronization are assumed. The CoS1 slot performance within ENR is shown in Figure 5.9. In this figure, both the specified and the proposed coding are simulated. It is obvious that the specified coding RS$(15, 11, 4)$ + CC(3/4) does not introduce a considerable coding gain compared to the uncoded curve. However, by using the proposed stronger CC of rate (1/2), the performance of a CoS1 slot approaches the recommended BER of 10^{-7}. Similarly to the AWGN, for short slot lengths, CC has the same performance as the concatenated coding.

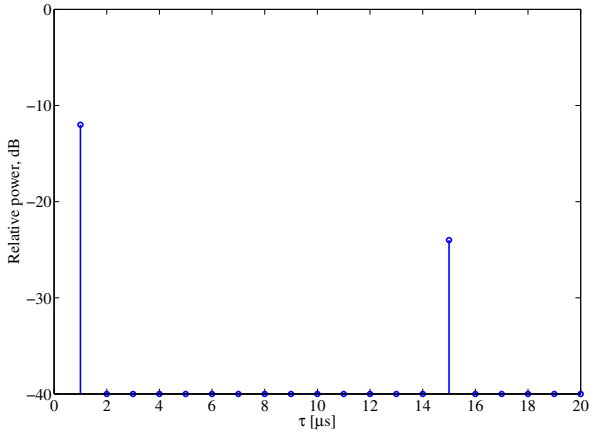

Figure 5.8: ENR channel power delay profile.

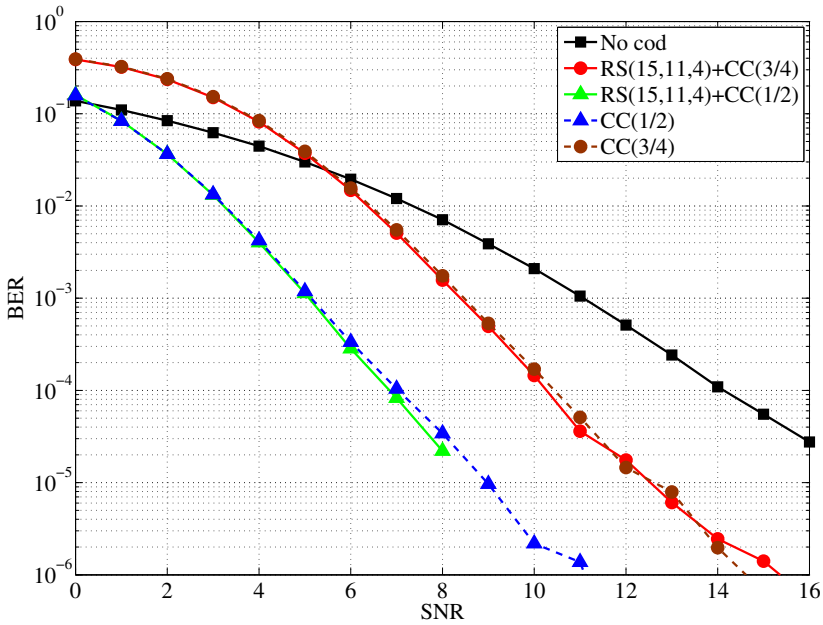

Figure 5.9: CoS1 slot: coded ENR, specifications vs. proposed coding.

The specified and proposed coding for the CoS2 slot under the ENR channel are simulated next. Figure 5.10 shows the bad performance of the specified concatenated coding RS$(31, 23, 5)$ and CC$(3/4)$. Even when using the proposed stronger CC of rate $(1/2)$, there is an error floor of BER $= 10^{-5}$. Because there is one training sequence for each CoS2 slot, the estimated channel impulse response $\hat{h}_{rx}$ is not valid for the entire 6.66 ms duration of the CoS2 slot, and thus the severe degradation in performance is observed.

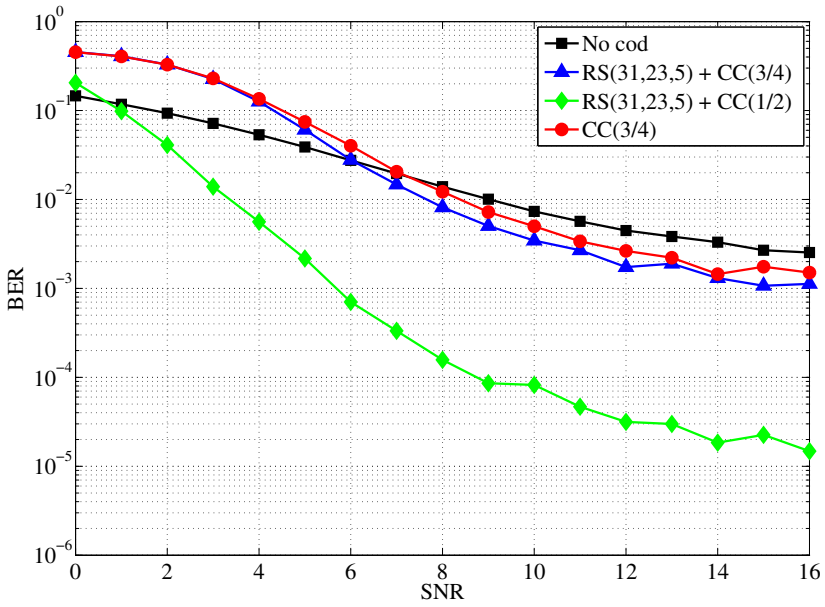

Figure 5.10: CoS2 slot: coded ENR, specifications vs. proposed coding.

To overcome this degradation, the CoS2 burst structure is next considered. However, the LDACS2 specification defines the usage of only one training sequence for either a slot or a burst, regardless of their lengths. Considering a normal GSM burst of 0.5 ms, there is one training sequence per each burst. Since the LDACS2 channel estimation and equalization is similar to the GSM except for the slot length, an adaptation is proposed to the burst structure. Considering a CoS2 burst of length 66.6 ms, this burst is 133 times the length of a GSM burst. Hence it is suggested to insert one training sequence for each 6.66 ms part of a CoS2 burst. Thus, for a CoS2 burst of 66.6 ms, 10 training sequences are inserted. Thus the estimated channel is only used for each 6.66 ms part of the entire burst. This approach is implemented in the rest of the simulations, whenever a burst structure is simulated.

The performance of a CoS2 burst of 66.6 ms length is shown in Figure 5.11. Both the specified and the proposed coding are simulated under the ENR channel. Due to the longer length of the burst, the RS symbol interleaver can interleave the adjacent symbols over multiple RS codewords. Thus, a burst error will not affect two adjacent codewords and hence a considerable performance enhancement is observed. Using the proposed CC of rate $(1/2)$ concatenated with RS$(31, 23, 5)$, there is a gain of about 6 dB compared to the specified coding.

The influence of the CoS2 burst length and the BER performance using the specified coding is shown in Figure 5.12. Obviously, as the burst length increases, higher coding

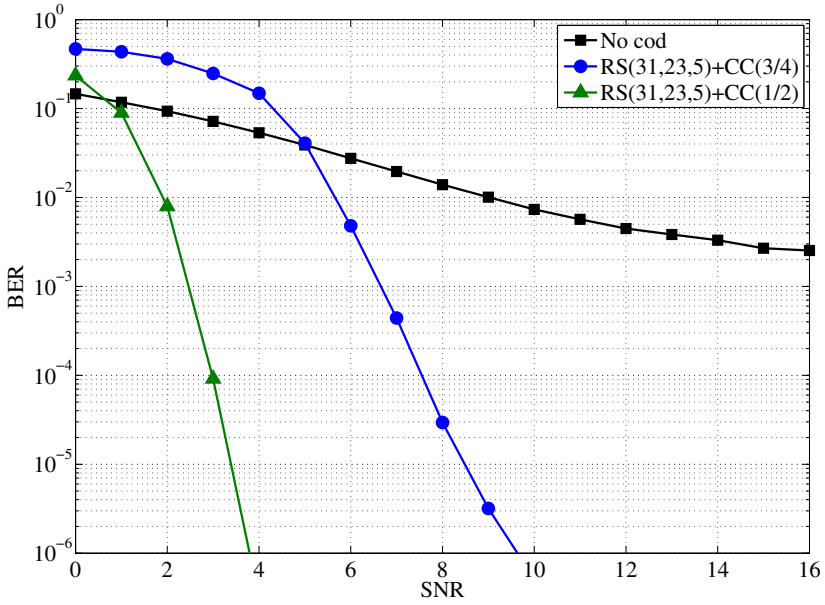

Figure 5.11: CoS2 burst: coded ENR, specifications vs. proposed coding.

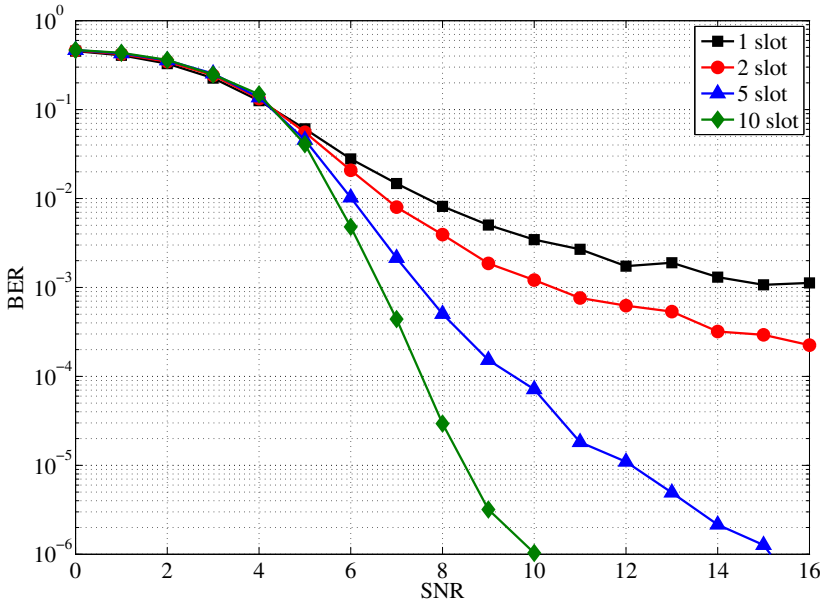

Figure 5.12: CoS2 burst size influence, ENR, specified coding: RS$(31, 23, 5)$ + CC(3/4).

gain can be achieved. Using the proposed coding of CC(1/2) for the same burst size and the same ENR channel, further performance improvement is achieved, as seen in Figure 5.13.

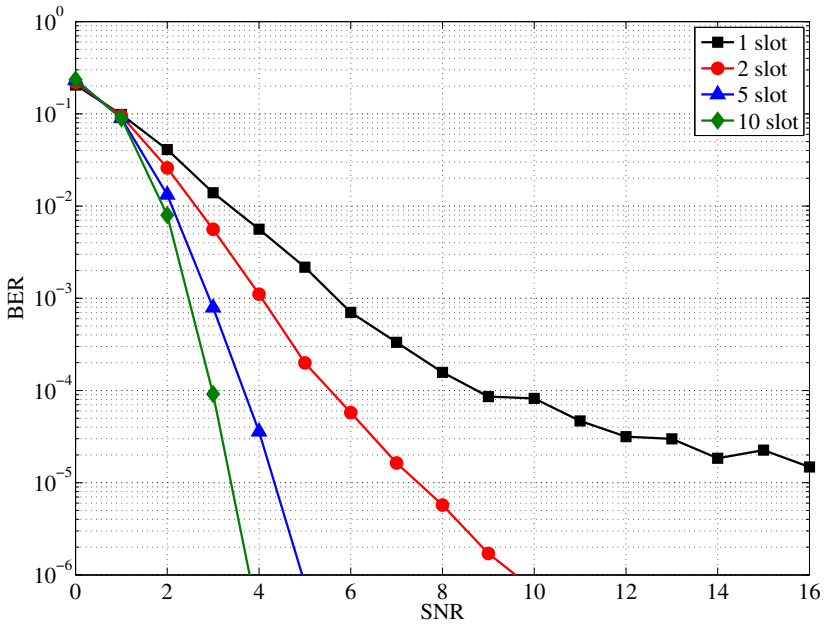

Figure 5.13: CoS2 burst size influence, ENR, proposed coding: RS$(31, 23, 5)$ + CC$(1/2)$.

The UP burst performance in coded ENR is depicted in Figure 5.14. Similar to the coded AWGN, the performance of a UP burst of length 13.3 ms with single training sequence per burst resembles the performance of a single CoS2 slot in the ENR channel. This is because of the similar structure of both of the CoS2 and UP bursts for the same burst length.

This work proposes another possibility to enhance the system performance in the ENR channel is to introduce more training sequences per a single slot. This makes $\hat{h}_{rx}$ valid only for part of the slot and then a new $\hat{h}_{rx}$ is estimated for the next part. The effect of increasing the number of training sequences per the slot is shown in Figure 5.15. Although it enhances the performances significantly, it reduces the system capacity by introducing extra redundant bits into the slot. The same discussion applies to the UP burst but it is not simulated due to its similarity with CoS2 slot.

5.1.4 LDACS2 Performance in the the TMA Channel

The TMA channel model is different from ENR in that it has less Doppler shift due to lower speed of the AC. The maximum experienced Doppler shift is 500 Hz. However, the TMA power delay profile follows an exponential decay (Figure 5.16), which

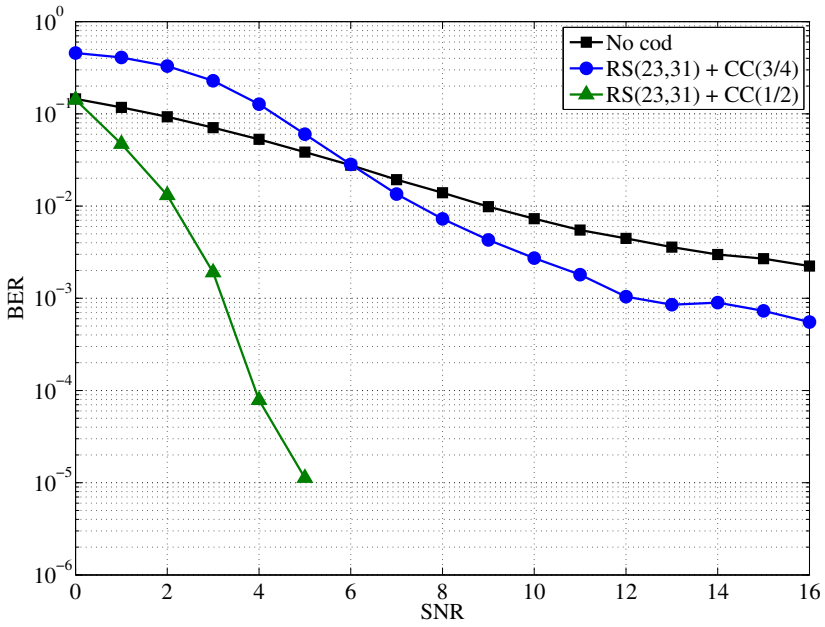

Figure 5.14: UP burst: coded ENR, specifications vs proposed coding.

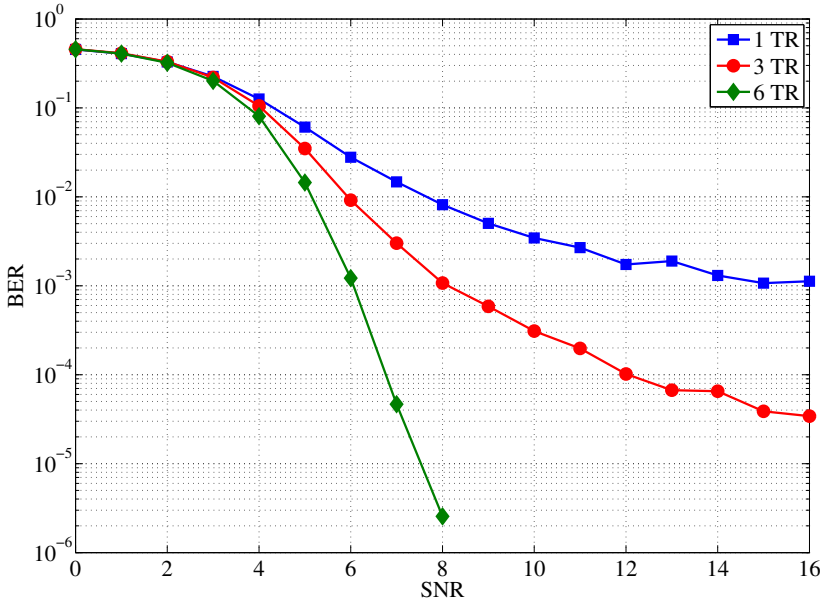

Figure 5.15: Number of training sequences per a single CoS2 slot, ENR, specified coding: RS$(31, 23, 5)$ + CC$(3/4)$.

indicates that the LDACS2 performance suffers more degredation in the TMA channel than in the ENR channel. The CoS1 slot performance under the TMA channel using the specification coding of CC$(3/4)$ is shown in Figure 5.17. Since the burst errors are beyond the capability of the coder, the decoder decodes the codewords wrongly, and thus the performance is worst than the non-coded case. Even with the proposed

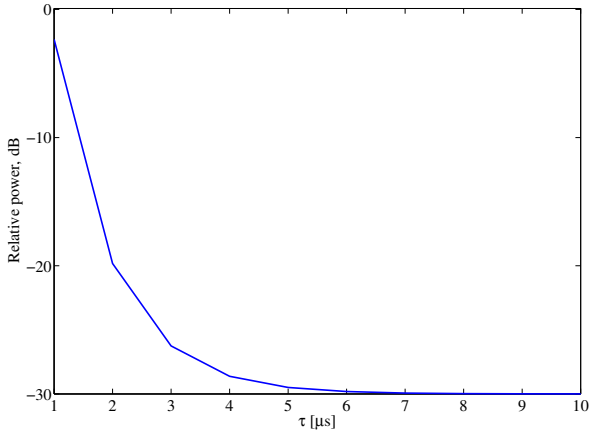

Figure 5.16: TMA channel power delay profile.

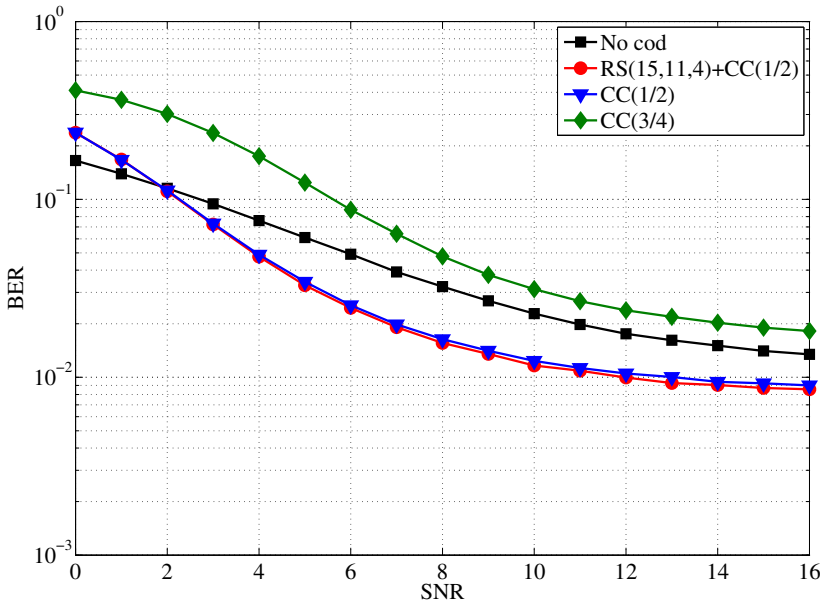

Figure 5.17: CoS1 slot: coded TMA, specifications vs. proposed coding.

strong coding of CC(1/2), there is an error floor of BER = 10^{-2}. CoS2 slots and UP burst show similar performance in the TMA channel.

Considering the CoS2 burst structure of 66.6 ms using the specified coding of RS$(31, 23, 5)$ with a CC(3/4), the performance is very poor and is comparable to the non-coded case, as shown in Figure 5.18. However, using the proposed coding of RS$(31, 23, 5)$ with a CC(1/2), the performance significantly enhances, as shown is the same figure.

In addition to the burst structure, increasing the the number of training sequences will also enhance the performance, as seen in Figure 5.15.

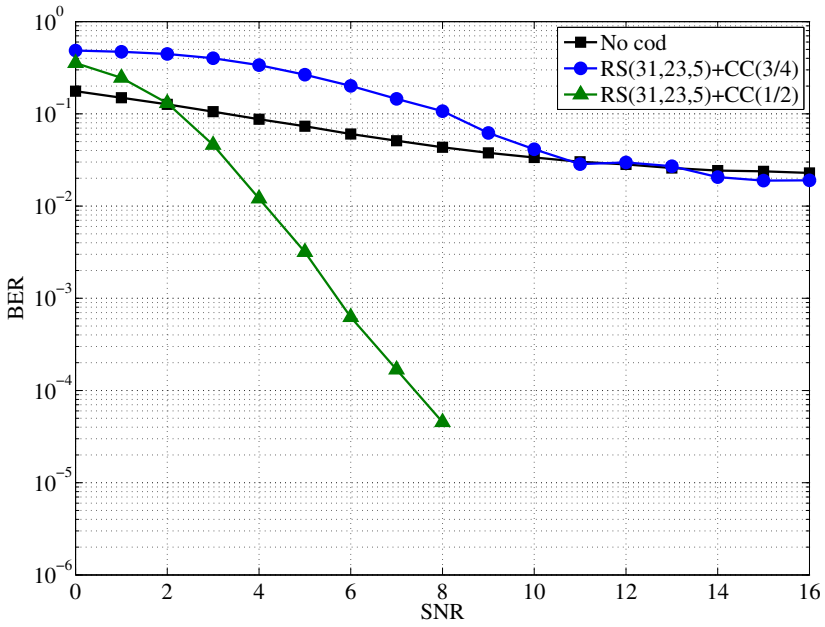

Figure 5.18: CoS2 burst: TMA, specifications vs. proposed coding.

5.1.5 DME Co-site Interference

In this section, the performance of LDACS2 against co-site interference from a DME interrogator is evaluated. A UP burst of length 66.6 ms is chosen and an AWGN channel is assumed. One training sequence is inserted every 6.66 ms. The LDACS2 receiver is assumed to receive data from the LDACS2 GS while a DME interrogator sends pulses at a rate of 150 Pulse Pairs Per Second (ppps). To mitigate the co-site interference, the LDACS2 receiver is assumed to blank its received signal whenever high power pulses are detected. This approach is known as pulse blanking. At a rate of 150 PPPS, a maximum of one DME pulse is expected to occur every 6.66 ms, i.e., 10 DME pulses within the simulated UP burst. Each DME pulse pair has a duration of approximately 17μs, which is equivalent to 5 bits of the received data is to be blanked. The LDACS2 receiver performance against DME co-site interference is shown in Figure 5.19. The LDACS2 performance hardly degrades due to the DME interference. This is an important feature of LDACS2 in that it is possible to deploy LDACS2 while DME interrogators are in service.

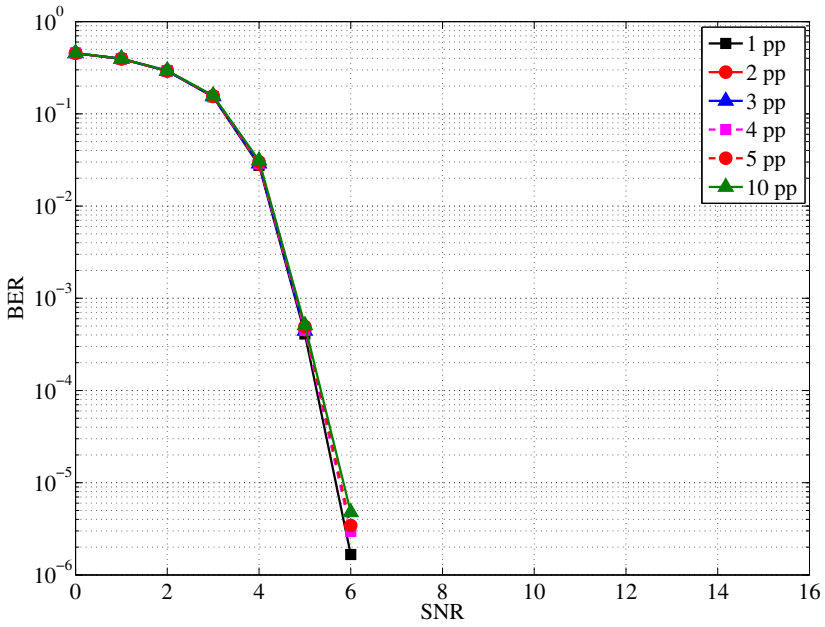

Figure 5.19: UP burst performance against co-site DME, AWGN, specified coding: RS$(31, 23, 5)$ + CC$(3/4)$.

5.1.6 Time and Frequency Error Performance

In this section, the LDACS2 robustness against time synchronization errors as well as frequency estimation errors are tested. Synchronization errors are assumed to occur whenever the start of the burst (UL or DL) is shifted in time. Although the LDACS2 specification assumes a very accurate synchronization, errors have to be tested. For this reason, a CoS2 burst is considered and ENR channel is assumed. The SNR is kept fixed at 10 dB and the synchronization error is introduced in time to the input of the channel estimator as a Gaussian process with zero mean and a standard deviation $\sigma_{\Delta t}$ defined as

$$\sigma_{\Delta t} = \sigma_t \cdot T_b, \tag{5.6}$$

where σ_t is the standard deviation of the error. $\sigma_{\Delta t}$ is then rounded to the nearest integer and added to the value k that represents the actual start of the burst, as calculated in (4.10).

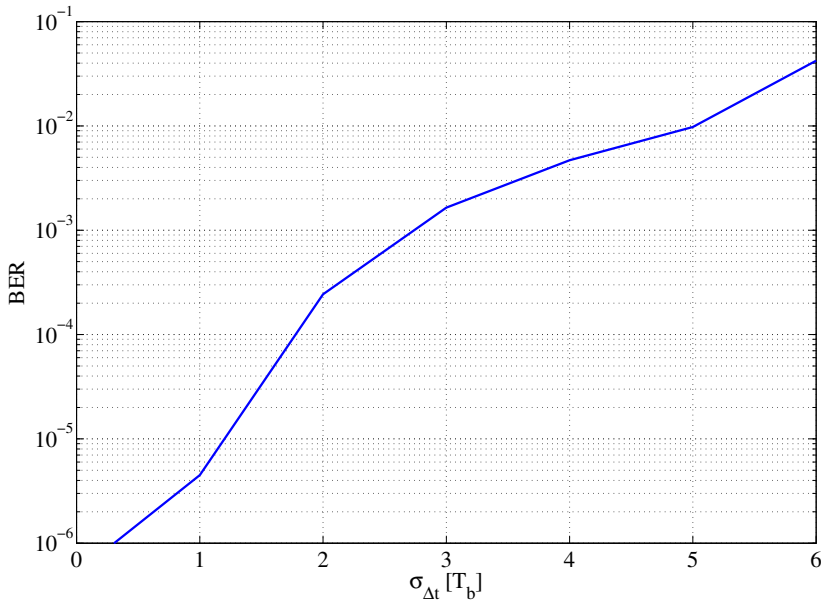

Figure 5.20: CoS2 burst performance against synchronization error, AWGN, SNR = 10 dB, specified coding: RS$(31, 23, 5)$ + CC$(3/4)$.

The simulation results are shown in Figure 5.20. Since the channel estimator tracks the starting of the burst (as seen in Chapter 4), the simulation curves show acceptable performance of the system up to an error variance of $3T_b$. In reality, the synchronization error occur infrequently because the LDACS2 GS forces the AC to stay in synchronization on a timely basis (similar to the GSM where the synchronization burst is defined).

LDACS2 robustness against frequency estimation error is also tested. To estimate the exact carrier frequency F_c, f_D should be exactly known at the receiver to compensate for the shift in F_c. The error in f_D estimation leads to an error in F_c synchronization. The standard deviation of the error introduced in the frequency estimation $\sigma_{\Delta f}$ is defined as

$$\sigma_{\Delta f} = \sigma_f \cdot F_c, \tag{5.7}$$

where σ_f is the standard deviation of the error. After generating $\sigma_{\Delta f}$, it is added to f_D in the receiver to simulate the error in the frequency estimation. The system performance is shown in Figure 5.21. Unlike time synchronization error, LDACS2 shows high sensitivity to errors in frequency estimation. An error in frequency estimation

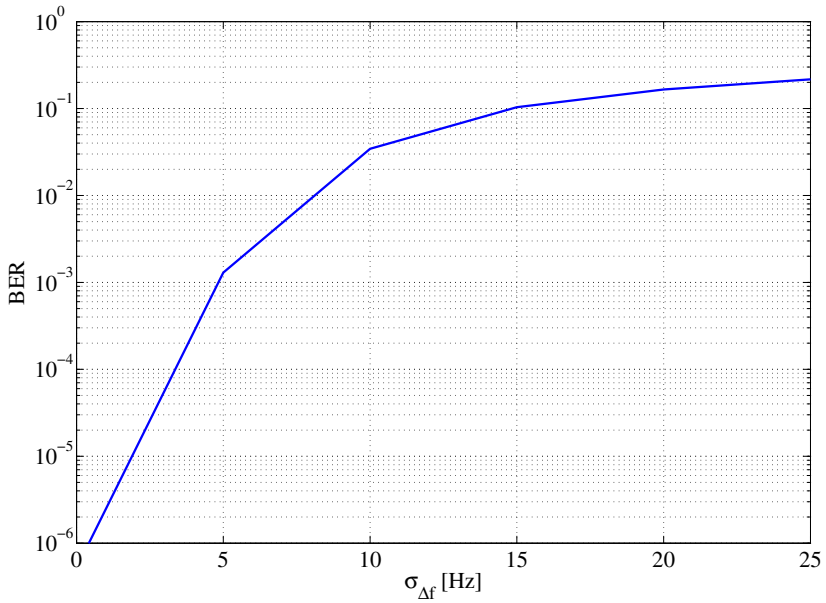

Figure 5.21: CoS2 burst performance against Frequency error, ENR channel, SNR = 10 dB, specified coding: RS$(31, 23, 5)$ + CC$(3/4)$.

of 15 Hz degrades the BER to 10^{-1}. Thus very accurate frequency synchronization algorithms are required at the LDACS2 receiver.

5.2 LDACS2 Capacity

In this section, the LDACS2 capacity is analyzed. A typical LDACS2 frame is considered and the UL and DL information bit rates R_i are calculated. In addition, the effect of inserting extra training sequence per a slot on the information bit rate is investigated.

As known, the gross bit rate R_b, defined in Chapter 1, is different from the actual information rate R_i. R_b is defined as the rate at which all the bits in the slot are transmitted per second, including redundant bits and guard bits. Obviously, R_i is smaller than R_b because there are always redundant bits to be added. To evaluate the LDACS2 capacity in terms of R_i, a high density cell is considered. The scenario assumes the existence of 204 AC per cell, which is the maximum number of ACs to be supported by LDACS2. The length of each section and the according number of slots are given in Table 5.1.

According to this configuration, the offered R_i will vary according to R_c, burst length (UP and CoS2) and the number of training sequence per burst. Table 5.2 summarizes the UL and DL information rate for different parameters.

Table 5.1: High density LDACS2 scenario

Section	Slot/section	Slot length (bits)
UP1	14	3612
CoS1	204	300
LoG2	4	902
UP2	14	3612
CoS2	58	1806

Table 5.2: LDACS2 capacity example

LDACS2	Coding	Slot/burst	R_i [kbps]
Overall	CC(3/4)	1	115.2
UL	CC(3/4)	1	35.3
DL	CC(3/4)	1	80
Overall	CC(1/2)	1	73.1
UL	CC(1/2)	1	22.4
DL	CC(1/2)	1	59
Overall	CC(3/4)	2	108.7
UL	CC(3/4)	2	29
DL	CC(3/4)	2	79.7
Overall	CC(3/4)	5	107.1
UL	CC(3/4)	5	24.6
DL	CC(3/4)	5	82.5
Overall	CC(3/4)	10	107.9
UL	CC(3/4)	10	25.6
DL	CC(3/4)	10	82.3

It can be seen that using the moderate CC(3/4) coding, the overall R_i is 115 kbps for both the UL and DL. A comprise between the UL and DL information rates could be achieved by modifying the length of UL and DL section to cope with different traffic requirements. However, this code rate is seen to perform badly in aeronautical channels and hence when using a stronger CC of rate (1/2), the overall LDACS2 capacity drops to 73 kbps. Another option is to transmit data in bursts spanning multiple slots (for CoS2 and UP sections only). It is noted that, increasing the burst size to 5 enhances the capacity as well as the performance (as seen in Section 5.1.3). Even increasing the burst size to 10 slots will maintain the same information rate but enhances the

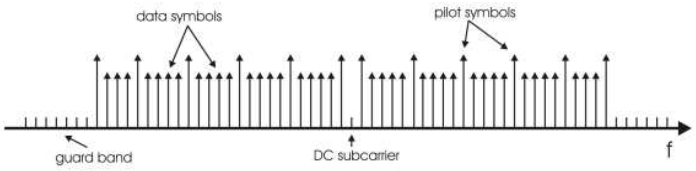

Figure 5.22: LDACS1 FL structure, one OFDM symbol in frequency domain [33].

performance further. One training sequence has been inserted for each slot to enhance the performance. However, it should be mentioned that when using a burst structure, the number of users that can simultaneously access those bursts decreases significantly. On the other hand, for all scenarios, the number of users that can access the CoS1 section remains unchanged and thus critical messages are guaranteed to be exchanged at the same rate.

5.3 LDACS2 vs. LDACS1 Performance

In this section, the LDACS1 is described in summary. The main physical parameters are illustrated as well as the channel coding and modulation. Then, performance comparision between the LDACA1 and LDACS2 is carried out.

5.3.1 LDACS1 Parameters

The LDACS1 physical layer is an OFDM-based modulation, designed to operate in the L-band. The LDACS1 FL is a continuous OFDM transmission, while the LDACS1 RL is based on OFDMA-TDMA. This allows different users to access the burst on demand. The LDACS1 FL transmission description is shown in Figure 5.22. It can be seen that guard times are used on both sides of the spectrum, to prevent out-of-band radiation. The LDACS1 RL transmission structure is shown in Figure 5.23. Each user has its assigned time slot and sub-carrier. The time-frequency structure is called tile. Table 5.3 summaries the main parameters used both in the FL and RL.

The LDACS1 has the same concatenated coding schemes, i.e., the outer coder is RS and the inner coder is CC. The FL frame of 2184 bits is coded with RS$(101, 91, 5)$ concatenated with CC(1/2). The RL data segment of 672 bits is coded with RS$(98, 84, 7)$ concatenated with CC(1/2). The encoded bits, together with redundancy, headers and

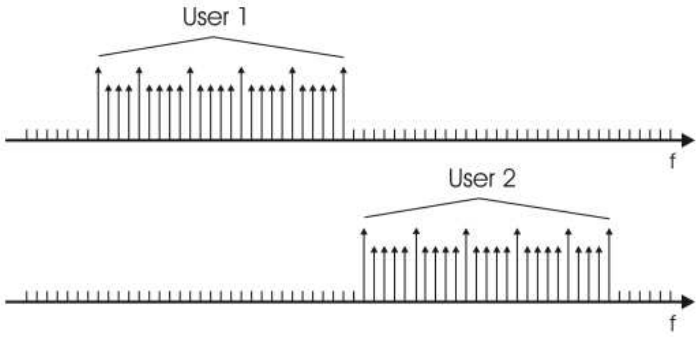

Figure 5.23: LDACS1 RL structure [33].

Table 5.3: LDACS1 OFDM parameters

Parameter	Value
FFT size	64
Sampling time	1.6 μs
Sub-carrier spacing	9.76 kHz
Useful symbol time	102.4 μs
OFDM symbol time	120 μs
Lower frequency guard sub-carriers	7
Higher frequency guard sub-carriers	6
FL structure	frame
RL structure	tile
FL capacity	2442 bits/frame
RL capacity	134 symbols/tile

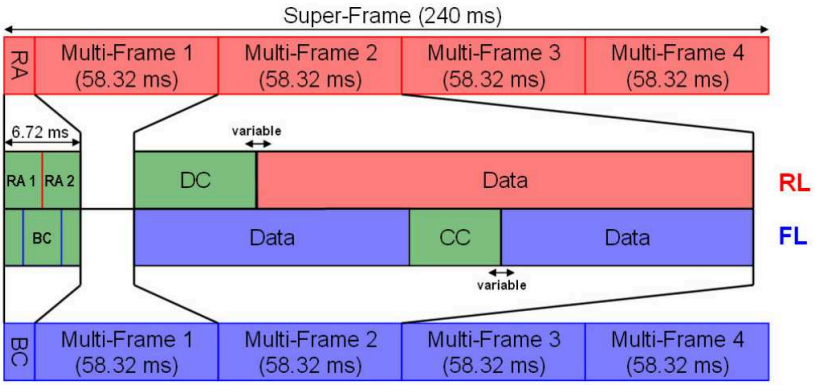

Figure 5.24: LDACS1 super frame [33].

trailers are formed into a Super-Frame (SF) structure. Each SF is 240 ms and corresponds to 2000 OFDM symbols. The SF is shown in Figure 5.24. Finally, each frame is then modulated.The LDACS1 supports Gray-mapped QPSK, 16QAM and 64QAM.

5.3.2 Performance Comparison

In this section, a comparison between LDACS1 and LDACS2 is carried out. The LDACS1 is an OFDM-based system, which has an effective channel bandwidth of 500 kHz. For a fair comparison between both systems, the received power P_r is assumed to be equal for both, LDACS1 and LDACS2. The linear SNR is defined as [28]

$$\mathrm{SNR}_l = \frac{P_r}{N_0 B}, \tag{5.8}$$

where B is the bandwidth of the baseband signal and $N_0 B$ is the total noise power within the passband signal bandwidth $2B$. Then for LDACS1, the SNR_l is written as

$$\mathrm{SNR}_{l1} = \frac{P_r}{N_0 \cdot 500\ \mathrm{kHz}}. \tag{5.9}$$

The SNR_l for LDACS2 is written as

$$\mathrm{SNR}_{l2} = \frac{P_r}{N_0 \cdot 200\ \mathrm{kHz}}. \tag{5.10}$$

Then the relationship is

$$\mathrm{SNR}_{l2} = 2.5 \cdot \mathrm{SNR}_{l1}, \tag{5.11}$$

and in the logarithmic dB scale, the relationship is written as

$$\mathrm{SNR}_2 = 4 + \mathrm{SNR}_1. \tag{5.12}$$

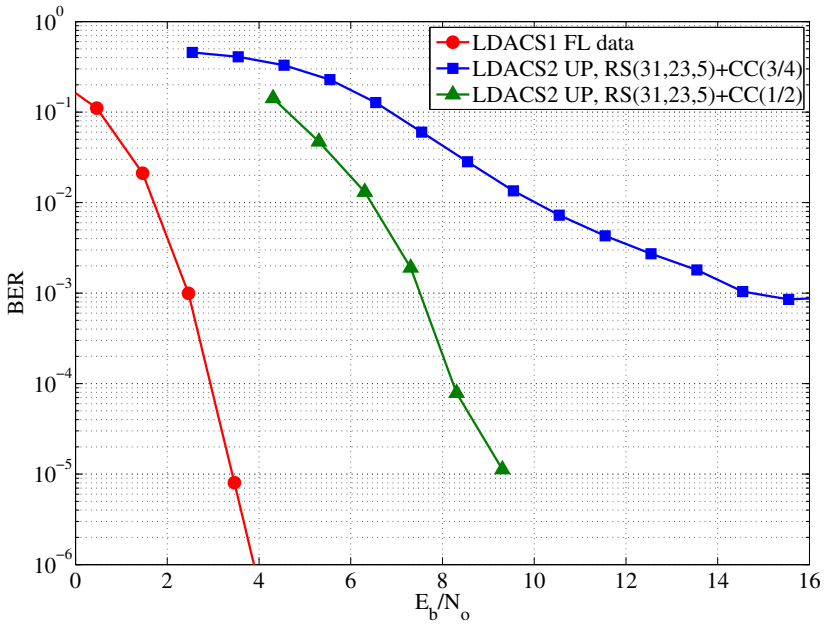

Figure 5.25: LDACS1 FL data frame, RS$(101, 91, 5)$ + CC$(1/2)$ vs. LDACS2 UP burst (specifications vs. proposed coding).

(5.12) shows that the SNR of LDACS2 is larger than that of LDACS1 by 4 dB, due to the smaller bandwidth of LDACS2 compared to LDACS1.

To compare both LDACS1 and LDACS2, E_b/N_0 in logarithmic scale (dB) is used instead of the SNR. The relation between (E_b/N_0) dB and the SNR is given by

$$(E_b/N_0)\ \text{dB} = \text{SNR} - 10\log R_c. \tag{5.13}$$

The LDACS1 Forward-Link (FL) data frame [33], which has 2184 information bits and the LDACS2 UP burst are simulated and compared in Figure 5.25 for the ENR channel.

Clearly, the LDACS1 performance is better than LDACS2 for the UL, using the specification coding. This is due to the stronger coding of LDACS1 compared to LDACS2. Besides, the LDACS1 frame has several pilot symbols distributed over time and frequency, which makes the channel estimation more accurate in fast fading channels. Even with the proposed stronger coding, LDACS1 performance still better than LDACS2.

The performance of an LDACS1 Reverse-Link (RL) data segment of 672 information bits is next compared to the LDACS2 CoS2 slot in Figure 5.26. The performance of LDACS1 RL is also better than that of LDACS2 DL, even with the proposed stronger coding.

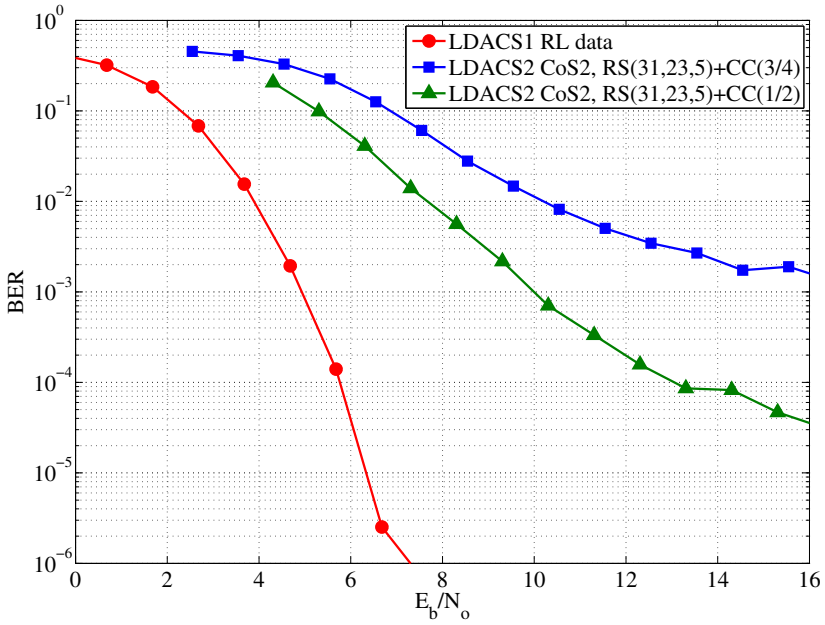

Figure 5.26: LDACS1 RL data segment, RS$(98, 84, 7)$ + CC$(1/2)$ vs. LDACS2 CoS2 slot (specifications vs. proposed coding).

6 Conclusions

In this master thesis, the LDACS2 proposal is studied. The LDACS2 model is implemented in a software simulator. Its performance is evaluated for the first time and important results are obtained. Those results can be used in the final selection of one of the two proposals for the future aeronautical communication system.

6.1 Implementaion

One of the main tasks of this work is the analysis of the LDACS2 proposal specifications. Since the LDACS2 transmitter and receiver parameters are not mentioned in the specifications, they are first investigated and determined. Due to its basic principle as a GMSK transmission concept, the LDACS2 transmitter is built similar to the GSM specifications. Then, channel coding, multiplexing and modulation are implemented, tested and verified according to the LDACS2 frame structure. The LDACS2 receiver is then implemented. Successful demodulation is achieved by using channel equalization algorithm known from the GSM. The LDACS2 receiver is also tested for the correct demodulation of the received signal waveform. The channel decoding is also implemented and tested.

Adapting the aeronautical channel models as described in [27] is the next important task of this thesis. The channel model implementation is adapted to fit the TDMA environment of the LDACS2.

The other accomplished task is simulating the LDACS2 within the aeronautical channel models environments. The simulations are done using the MATLAB simulator. Taking into account the long LDACS2 burst compared to the GSM, many implementation techniques have to be done to cope with time synchronization, channel estimation and channel equalization. Since the GSM specification supports low speed mobility,

the great challenge was to adapt channel equalization to cope with very high speeds experienced in aeronautics environments.

Further enhancements on the system are proposed and validated through simulations. Those include the insertion of extra training sequences, a longer burst structure and stronger coding.

6.2 Results

The simulation results of LDACS2 show the plausibility of the system deployment. The LDACS2 performance using the specified code rate and slot structure showed a poor performance. However, considerable enhancements on the system performance are proven using stronger coding with the same slot structure. However, with stronger codes, the information bit rates are decreased. On the other hand, introducing more training sequences per single burst while maintaining the specified code rate achieves the same performance, as shown by the simulation results.

A third possibility is to transmit the data in bursts spanning multiple slots instead of single slot. This has the advantage of encoding longer messages and then the symbols are interleaved further apart across the burst, which minimizes the effect of burst errors. It has been shown that a burst of up to 5 basis slots with the specified CC with $R_c = 3/4$ performs the same as single slot structure with stronger CC with $R_c = 1/2$. Thus, the information bit rate is kept at maximum while keeping the system performance at acceptable level.

The simulation results also showed that for short-length slots, such as CoS1 slots, it is sufficient to use only CC instead of concatenated codes (RS with CC). Simulations showed that there is no coding gain when using concatenated codes compared to single code.

The simulations also show that the LDACS2 is robust against time synchronization errors that occur at the receiver. The system shows an acceptable performance.

However, the simulations showed that the LDACS2 is less robust against errors in frequency estimation.

The overall information rate, however, is low compared to nowadays offered bit rates. As illustrated in the implementation example, for a cell with a maximum capacity of 204 AC, the offered bit rate cannot exceed 115 kbps for both the UL and DL. This shows that the LDACS2 system support basic data communications, like navigation and traffic control. There is even the possibility of supporting voice using the existing structure or a separate voice channel. However, to increase the offered information rate, many solutions on the system are to be introduced. One of those is to aggregate channels to have higher information data rates, as suggested in the specifications.

6.3 Design Drawbacks

Since the LDACS2 slot relies on the training sequence to estimate the channel, the currently specified training sequence position is not practical. To be able to estimate the accurate channel impulse response, the training sequence should be placed in the middle of the slot, similarly to the GSM. Besides, long slots (CoS2 and UP) have bad performance because of the single trainging sequence dedicated to the entire slot. This leads to bad performance for fast fading channels, as seen in Section 5.1.3.

Another design drawback is the location of the CRC, which is outside the coded data. For the receiver to be able to determine transmission errors that pass the FEC coding, the CRC should also be protected by coding. Thus, it is recommended that the CRC is coded together with the user data.

The LDACS2 proposal is a half-duplex system. To increase the offered R_i, full-duplex implementation is recommended for simultaneous access of both the AC and the GS. This requires channel aggregation among at least two channels. The full-duplex system will then offer higher data rates according to the number of aggregated channels.

6.4 Future Work

Further enhancements could be introduced into the LDACS2 to increase its information rate. General Packet Radio Service (GPRS), High-Speed Downlink Packet Access (HSDPA) and Enhanced Data rates for GSM Evolution (EDGE) data services used in the GSM can be applied. The 8PSK modulation scheme applied in the EDGE, for

example, can be implemented on the top of the existing single carrier modulation in LDACS2, providing higher bit rates than that of the GMSK modulation. The frame structure, however, needs to be adapted according to the implemented services.

To enhance the LDACS2 BER performance against aeronautical channels, the usage of more efficient codes is suggested. Turbo-codes [34] are recommended. Those codes perform better and less sensitive to puncturing than the convolutional codes. They approach the Shannon limit for channel capacity and thus will increase the offered R_i. However, Turbo-codes are not suitable for short length slots, like the CoS1 slot. Block codes can also be implemented. However, there is a trade-off between their reliability against channel impairments and their complexity. Hybrid Automatic Repeat Request (hybrid ARQ) is also another potential to enhance the LDACS2 performance against errors. The principle is to send the redundancy bits only when the message is detected as corrupted by the CRC. However, the trade-off of this technique is lower system throughput. Validating the performance of those codes and techniques is then through simulations is necessary before deployment.

Acronyms

LDACS1 L-band Digital Aeronautical Communications System, Type1 1

LDACS2 L-band Digital Aeronautical Communications System, Type2 1

AWGN Additive White Gaussian Noise 1

FCS Future Communication Study 1

ICAO International Civil Aviation Organization 1

MAC Medium Access Control 1

BER Bit Error Rate 1

ARS Aeronautical Radio-navigation Services 2

FDMA Frequency Division Multiple Acces 2

TDMA Time Division Multiple Access 2

AMACS All Purpose Multichannel Aviation Communication System 2

ATC Air Traffic Control 4

AOC Airline Operational Control 4

DLS Data Link Sublayer 5

LSS LDACS2 Service Sublayer 5

LME Link Management Entity 6

LML Link Management Layer 6

TDD Time Division Duplexing 6

LDL L-band Digital Link 7

VDL VHF Digital Link 7

GMSK Gaussian Minimum Shift Keying 7

MSK Minimum Shift Keying 7

QPSK Quadrature Phase Shift Keying 7

FSK Frequency Shift Keying 8

ISI Inter Symbol Interference 9

NM Nautical Mile . . . 9

AC Aircraft . . . 10

GS Ground Station . . . 10

RS Reed Solomon . . . 17

CRC Code Redundancy Check . . . 17

RTZ Return-to-Zero . . . 20

MLSE Maximum Likelihood Sequence Estimator . . . 23

PSD Power Spectrum Density . . . 25

LOS Line of Sight . . . 27

ACF Autocorrelation Function . . . 28

WSSUS Wide-Sense Stationary Uncorrelated Scatterers . . . 28

ENR En-Route . . . 30

KTAS Knots True Airspeed . . . 30

TMA Terminal Maneuvering Area . . . 32

RTT Round Trip Time 33

NRZ Non-Return-to-Zero 45

SNR Signal-to-Noise Ratio 45

GF Galois Field 47

DL Down Link 54

UL Up Link 57

GPRS General Packet Radio Service 77

HSDPA High-Speed Downlink Packet Access 77

EDGE Enhanced Data rates for GSM Evolution 77

ppps Pulse Pairs Per Second 65

Bibliography

[1] Najett Neji, Raul de Lacerda, Alain Azoulay, Thierry Letertre, Olivier Outtier, *Interference Analysis for the Future Aeronautical Communication System*. IEEE, 2009.

[2] *L-DACS2 System Definition Proposal: Deliverable D2*. European Organozation for the Safety of Air Navigation, 2009.

[3] Ulrich Epple, Michael Schnell, *Overview of Interference Situation and Mitigation Techniques for LDACS1*. German Aerospace Center (DLR), 30th Digital Avionics Systems Conference, October, 2011.

[4] Raj Jain, Fred Templin, Kwong-Sang Yin, *Analysis of L-Band Digital Aeronautical Communication Systems: L-DACS1 and L-DACS2*.

[5] *What is GMSK Modulation - Gaussian Minimum Shift Keying*. Resource and analysis for electronics engineers, Radio-Electronics.com.

[6] *Modelling an Airline Operations Control*. Nicolas Pujet, Eric Feron, International Center for Air Transportation, Massachusetts Institute of Technology, Cambridge MA. December, 1998.

[7] Schwartz M., *Mobile Wireless Communications*. Cambridge University Press, 2005.

[8] Fred Kostedt, James C. Kemerling, *Practical GMSK Data Transmission*. MX-COM, INC, 1998.

[9] *Release Note Recommendation GSM 05.04 Modulation*. ETSI/TC SMG, March 1992.

[10] Arne Norre Ekstrøm, Jan H. Mikkelsen, *GSMsim A MATLAB Implementation of a GSM Simulation Platform*. Institute of Electronic Systems, Division of Telecom-

munications, Aalborg University, December, 1997.

[11] *L-DACS2 Transmitter and Receiver prototype equipment specifications: Deliverable D3*. European Organozation for the Safety of Air Navigation, 2009.

[12] Schwartz M., *Information Transmission, Modulation, and Noise*. New York, McGraw-Hill., 4th edn, 1990.

[13] Murota, K., Hirade, K., *GMSK Modulation for Digital Mobile Radio Telephony*. IEEE Transactions on Communications, vol.29, no.7, pp. 1044- 1050, Jul 1981.

[14] Raj Jain, *Channel Models A Tutorial*. WiMAX Forum, Feb 2007.

[15] Bjørn A. Bjerke, John G. Proakis, K. Y. Martin Lee, Zoran Zvonar, *A Comparison of GSM Receivers for Fading Multipath Channels with Adjacent- and Co-Channel Interference*. IEEE JOURNAL ON SELECTED AREAS IN COMMUNICATIONS, VOL. 18, NO. 11, Nov 2000.

[16] Moe Rahnema, *Channel Equalization for the GSM System*. IEEE, 1996.

[17] Dapeng Hao, Sabah Badri-Hoeher, Peter Adam Hoeher, *Training Sequence Design for EDGE System with Dual Symbol Rate*. Information and Coding Theory Lab, Faculty of Engineering, University of Kiel, Germany.

[18] Vipin Pathak, *MLSE Based Equalization and Fading Channel Modelling for GSM*. Hughes Software Systems, Digital Signal Processing Group, Electronic City, Gurgaon, India.

[19] G. DAVID FORNEY, JR., *Maximum-Likelihood Sequence Estimation of Digital Sequences in the Presence of Intersymbol Interference*. IEEE Transactions on Information Theory, May 1972.

[20] Ungerboeck, G., *Adaptive Maximum-Likelihood Receiver for Carrier-Modulated Data-Transmission Systems*. IEEE Transactions on Communications, May 1974.

[21] Raymond Steele, *Mobile Radio Communications*. John Wiley and Sons, ltd., second edition, 1992.

[22] Bernard Sklar, *Rayleigh Fading Channels in Mobile Digital Communication Systems, Part I: Characterization*. Communications Engineering Services, IEEE Communication Magazine, July 1997.

[23] Jay M. Jacobsmeyer, P.E, *Introduction to Error-Control Coding*. Pericle Communications Company, 2004.

[24] John G. Proakis, Masoud Salehi, *Digital Communications*. McGraw-Hill Higer Education, Fifth Edition, 2008.

[25] Bernard Sklar, *Reed-Solomon Codes*.

[26] *Expected B-AMC System Performance*. Broadband Aeronautical Multi-Carrier Communications System, Frequentis AG, DLR, Paris Lodron Universitaet Salzburg, Mileridge Limited, 2007.

[27] *Software Implementation of Broadband VHF Radio Channel Models*. Broadband VHF Aeronautical Communications System Based on MC-CDMA, Frequentis GMBH, DLR, National Air Traffic Services and others, May 2006.

[28] Andrea Godlsmith, *Wireless Communications*. Standford University, 2005.

[29] Andreas F. Molisch, *Wireless Communications*. John Wiley and Sons Ltd., Second Edition, 2011.

[30] Holger Floehr, *Avionik und Flugsicherungstechnik*. Springer-Verlag Berlin Heidelberg, Second Edition, 2010.

[31] Matich, G.E., Reynolds, C.D., Lazare, F.J., MacBride, J., Hunter, S., *The United Kingdom Mode 3 VHF Data Link (VDL) Trials Final Report, Issue 1*. Project Report by GEC-Marconi Sensors Ltd, National Air Traffic Services Ltd, October 1996.

[32] Seiichi Sampei, *Application of Digital Wireless Technologies to Global Wireless Communications*. Prentice Hall PTR, Upper Saddle River, NJ 07458, 1997.

[33] *L-DACS1 System Definition Proposal: Deliverable D2*. European Organozation for the Safety of Air Navigation, 2009.

[34] Claude Berrou, Alain Glavieux, *Near Optimum Error Correcting Coding and Decoding: Turbo-Codes*. IEEE Transactions on Communications, Vol. 44, No. 10, October 1996.

[35] Paul C. P. Liang, Wayne E. Stark, *Algorithm for Joint Decoding of Turbo Codes and M-ary Orthogonal Modulation*. IEEE, ISIT, Sorrento, Italy, June 2000.

List of Figures

1.1 Evolution of aeronautical datalinks [4]. 2
1.2 Selection process of the final LDACS proposal [2]. 3
1.3 LDACS2 layers. 6
1.4 L_band spectrum usage. 7
1.5 MSK modulated signal [5]. 9
1.6 LDACS2 frame structure [2]. 10
1.7 Basic slot structure [2]. 10
1.8 UP slot, 3612 bits, 13.33 ms [2]. 12
1.9 CoS1 slot, 300 bits, 1.11 ms [2]. 12
1.10 CoS2 slot, 1806 bits, 6.66 ms [2]. 13
1.11 LoG2 slot, 902 bits, 3.33 ms [2]. 13

2.1 LDACS2 general transmitter structure. 16
2.2 MSK modulator fed with a sequence of ones. I lags Q by $\pi/2$. Each T_b increases the phase by $\pi/2$. 18
2.3 MSK modulator. 18
2.4 For the same binary sequence, GMSK phase is smoother than MSK. . . 20
2.5 GMSK vs. MSK Spectrum. High attenuation for GMSK spectrum after 200 kHz. 20
2.6 Pulse shaping function $\acute{g}(t)$ is limited to $3T_b$. 23
2.7 LDACS2 transmitter chain. 24

3.1 Large fading (shadowing) vs. small scale (multi-path) fading [14]. . . . 27
3.2 Multipath power delay profile example [14]. 27
3.3 En-route Doppler power spectrum follows a Gaussian distribution. . . . 31
3.4 Take-off landing Doppler power spectrum, following a Jakes distribution. 32
3.5 DME co-site interference. 33
3.6 DME pulse pair in time domain [3]. 34

4.1 LDACS2 receiver architecture. 36
4.2 Auto correlation function characteristics of the training sequence. . . . 38
4.3 Cyclic structure of the training sequence. 38
4.4 Trellis structure example for $L = 2$ and 2^L states. 43
4.5 The good, the bad and the awful error performance [22]. 46
4.6 RS BER vs. code rate trade-off [25]. 49
4.7 Concatenated channel coding for LDACS2. 49

5.1 Estimated channel impulse response at the channel estimator. 54
5.2 CoS1: non-coded AWGN. 55
5.3 CoS1: coded AWGN, specifications coding. 55
5.4 CoS1: coded AWGN (proposed coding). 56
5.5 CoS2 slot: coded AWGN (specifications coding). 57
5.6 CoS2 burst: coded AWGN (specifications coding). 57
5.7 UP burst: coded AWGN (specifications coding). 58
5.8 ENR channel power delay profile. 59
5.9 CoS1 slot: coded ENR, specifications vs. proposed coding. 59
5.10 CoS2 slot: coded ENR, specifications vs. proposed coding. 60
5.11 CoS2 burst: coded ENR, specifications vs. proposed coding. 61
5.12 CoS2 burst size influence, ENR, specified coding: RS$(31, 23, 5)$ + CC$(3/4)$. 61
5.13 CoS2 burst size influence, ENR, proposed coding: RS$(31, 23, 5)$ + CC$(1/2)$. 62
5.14 UP burst: coded ENR, specifications vs proposed coding. 63
5.15 Number of training sequences per a single CoS2 slot, ENR, specified coding: RS$(31, 23, 5)$ + CC$(3/4)$. 63
5.16 TMA channel power delay profile. 64
5.17 CoS1 slot: coded TMA, specifications vs. proposed coding. 64
5.18 CoS2 burst: TMA, specifications vs. proposed coding. 65
5.19 UP burst performance against co-site DME, AWGN, specified coding: RS$(31, 23, 5)$ + CC$(3/4)$. 66
5.20 CoS2 burst performance against synchronization error, AWGN, SNR = 10 dB, specified coding: RS$(31, 23, 5)$ + CC$(3/4)$. 67
5.21 CoS2 burst performance against Frequency error, ENR channel, SNR = 10 dB, specified coding: RS$(31, 23, 5)$ + CC$(3/4)$. 68
5.22 LDACS1 FL structure, one OFDM symbol in frequency domain [33]. . 70
5.23 LDACS1 RL structure [33]. 71
5.24 LDACS1 super frame [33]. 71

5.25 LDACS1 FL data frame, RS$(101, 91, 5)$ + CC$(1/2)$ vs. LDACS2 UP burst (specifications vs. proposed coding). 73
5.26 LDACS1 RL data segment, RS$(98, 84, 7)$ + CC$(1/2)$ vs. LDACS2 CoS2 slot (specifications vs. proposed coding). 74

List of Tables

1.1 LDACS2 frame parameters. 11
1.2 Channel bandwidth vs. various cell sizes. 14
1.3 Channel interference. 15

3.1 ENR channel model parameters. 31
3.2 Take-off landing channel model parameters. 33

4.1 LDACS2 coding parameters. 50

5.1 High density LDACS2 scenario 69
5.2 LDACS2 capacity example 69
5.3 LDACS1 OFDM parameters 71

Erklärung

Die vorliegende Arbeit habe ich selbstständig ohne Benutzung anderer als der angegebenen Quellen angefertigt. Alle Stellen, die wörtlich oder sinngemäSS aus veröffentlichten Quellen entnommen wurden, sind als solche kenntlich gemacht. Die Arbeit ist in gleicher oder ähnlicher Form oder auszugsweise im Rahmen einer oder anderer Prüfungen noch nicht vorgelegt worden.

Ilmenau, den 06. 12. 2012 Haider Adbulkarim

Unterschrift

Theses of the Master Thesis

1. The LDACS proposal will replace the analog AM in aeronautical communications. LDACS is proposed to operate in the L-band (950-1450) MHz.

2. There are two proposal standards: LDACS1 (based on OFDM) and LDACS2 (based on TDMA).

3. The LDACS2 simulator is implemented in MATLAB according to the specifications. The LDACS2 simulator is adapted from an existing GSM simulator

4. LDACS2 performance is evaluated against realistic aeronautical channel models. The results show moderate-to-poor performance using the specified coding rates and burst structure.

5. LDACS2 robustness against time and frequency estimation errors as well as DME co-site interference is simulated. The results show that the LDACS2 is robust against DME interference and timing errors and sensitive against frequency errors.

6. To enhance the system performance, stronger coding is proposed, extra training sequences to be inserted and longer bursts to be used. The simulations show significant improvement in LDACS2 performance for each case.

7. LDACS2 capacity is investigated using both the specified and the proposed coding. The investigations show that the throughput is capable to cover air traffic data services needs.

8. LDACS1 performance is compared to LDACS2. Simulations show that LDACS1 performs better than LDACS2.